Tampere University

Tomi Nieminen

SWAY REDUCTION OF FOREST MACHINE GRAPPLE USING INPUT SHAPING

Master of Science Thesis
Faculty of Engineering and Natural Sciences
Examiners: University instructor Veli-Pekka Pyrhönen
Asst. prof. Azwirman Gusrialdi
October 2023

ABSTRACT

Tomi Nieminen: Sway reduction of forest machine grapple using input shaping
Master of Science Thesis
Tampere University
Automation Engineering
October 2023

Fluent operation of forest machine is challenging task and requires plenty of training. Thus, development of partially or fully automated motions has become key interest. With automation, cognitive load of operators can be reduced and productivity and efficiency increased. Also, for inexperienced operators, the amount of training could be reduced. Furthermore, abrupt movements that cause swaying are typical for inexperienced operators, which may limit their productivity.

Input shaping is an open-loop method that prevents unwanted swaying by modifying the command signal before feeding it to the system. The performance of input shaping relies on the estimated values of natural frequency and damping ratio of the system. As a drawback, input shaping delays part of the operator command for attenuation purpose.

In this thesis, input shaping was implemented to a control system of a real forest machine and tested with slewing and crane tip near-far movements. The grapple model parameters, values of natural frequency and damping ratio were determined from measurements of the grapple swaying. According to measurements, grapple model was identified and input shaper designed to prevent swaying in the modelled frequency.

According to the test results, input shaping was capable of reducing major part of the swaying. However with slewing, it was noticed that performance is depending on how well actual velocity of specific movement is following the command velocity. Yet, the reduction of swaying with slewing movement was significant. With near-far movement, almost all of the swaying was attenuated.

Also, the effect of parameter uncertainty to swaying motion was tested by deviating the nominal values of natural frequency and damping ratio. In cases where $\pm 10\%$ error in natural frequency or five times smaller or higher damping ratio exists, input shaper was capable of reducing major part of the swaying and only small deterioration in performance was detected. In addition, the effect of grapple opening and rotation was tested causing only minor changes to the modelled natural frequency and damping.

Keywords: Input shaping, Feedforward control, Forest machine, Swaying, Grapple

TIIVISTELMÄ

Tomi Nieminen: Metsäkoneen kahmarin heilunnan vaimennus käyttäen input shaping -menetelmää
Diplomityö
Tampereen yliopisto
Automaatiotekniikka
Lokakuu 2023

Metsäkoneen sujuva käyttäminen on haastava tehtävä ja vaatii paljon harjoittelua. Tämän takia osittain tai kokonaan automatisoidut liikkeet ovat kiinnostuksen kohde. Automaation avulla kuljettajan kognitiivista kuormitusta pystytään vähentämään ja tuottavuutta ja tehokkuutta parantamaan. Myös vaadittavan harjoittelun määrää pystytään kokemattomien kuljettajien tapauksessa pienentämään. Kahmarin huojunta on yksi tekijä, joka rajoittaa työskentelyn tehokkuutta. Kokemattomilla kuljettajilla huojuntaa aiheuttavat äkilliset liikkeet ovat tyypillisiä.

Input shaping on menetelmä, jolla järjestelmän värähtely pyritään estämään. Se perustuu mallinnettuihin systeemin ominaistaajuuteen ja vaimmennussuhteeseen. Haittapuolena input shaping -menetelmä viivästää osaa kuljettajan antamasta ohjauskomennosta vaimentaakseen värähtelyä.

Tässä työssä input shaping -menetelmä toteutettiin metsäkoneen ohjausjärjestelmään ja sitä testattiin nosturin kääntö- ja kärjen eteen—taakse-liikkeiden kanssa. Kahmarin ominaistaajuus ja vaimennussuhde määriteltiin saatujen mittausten perusteella. Mittausten perusteella määritettiin myös kahmarin mallin sekä input shaping -menetelmän parametrit.

Tulokset osoittivat, että input shaping -menetelmä vaimentaa kahmarin heilahtelun lähes kokonaan. Kuitenkin kääntöliikkeen osalta huomattiin, että vaimennus riippuu siitä, kuinka hyvin järjestelmän nopeus seuraa kuljettajan ohjauskomentoa. Silti suurin osa kahmarin huojunnasta pystyttiin vaimentamaan myös kääntöliikkeen tapauksessa. Kärjen eteen—taakse-liikkeen kanssa kahmarin huojunta pystyttiin vaimentamaan pois lähes kokonaan.

Myös parametriepävarmuuden vaikutusta huojuntaan testattiin poikkeuttamalla ominaistaajuuden ja vaimennussuhteen arvoja niiden nimellisarvoista. Tapauksissa, joissa esiintyi ± 10 % virhe ominaistaajuudessa ja 5 kertaa suurempi tai pienempi vaimennussuhde, input shaping -menetelmä pystyi vaimentamaan suurimman osan kahmarin huojunnasta. Lisäksi kahmarin asennon vaikutus todettiin vaikuttavan vain vähän mallinnetuun ominaistaajuuteen ja vaimennussuhteeseen.

Avainsanat: input shaping, myötäkytkentä, metsäkone, huojunta, kahmari

PREFACE

The research of this thesis was both challenging and interesting. Especially, I want to thank Ponsse and Joni Backas for interesting topic and possibility to test the results with real forest machine. To be able to see the results in real life was rewarding. Also, thanks to Jari Korhonen who helped with the practical stuff related to testing.

Also, guidance of Veli-Pekka Pyrhönen through thesis and studies was invaluable. The inspiring way of teaching is something I value high. Also, big thanks to Azwirman Gusrialdi and Elham Kowsari with the feedback and help during thesis process.

Finally, I am grateful of my girlfriend and family who time to time gave something else to think about than thesis.

In Tampere, 10th October 2023

Tomi Nieminen

CONTENTS

GLOSSARY

BIBO	Bounded-input bounded-output
DC gain	Direct current gain
DOF	Degree-of-freedom
EI shaper	Extrainsensitive shaper
IMU	Inertial measurement unit
IS	Input shaping
ISE	Integral of squared error
LTI	Linear time invariant
MIMO	Multi-input multi-output
MISO	Multi-input single-output
MPC	Model predictive control
RM shaper	Reduced modification shaper
SIMO	Single-input multi-output
SISO	Single-input single-output
SLAM	Simultaneous localization and mapping
ZVD shaper	Zero-vibration-derivation shaper

LIST OF SYMBOLS

A, B, C, D	State space model matrices
A_i	Size of impulse i
C	Cosine term of residual vibration
$G_{u_i y_j}$	Transfer function from input i to output j
K	DC gain
L	Lagrangian
R, R_{dB}	Amplitude response
S	Sine term of residual vibration
T	Kinetic energy
V	Potential energy
$V(\omega_n, \xi)$	Residual vibration
V_{tol}	Tolerated residual vibration
ϵ	Modification error of RM shaper
$\mathbb{R}$	Real numbers
ω_d	Damped natural frequency
ω_n	Undamped natural frequency
ϕ	Phase response
τ	Time constant
τ_{θ_i}	Torque of joint i
θ_1	Parallel swaying angle
θ_2	Perpendicular swaying angle
ξ	Damping ratio
b_i	Damping coefficient of joint i
e	Actuating error
f	Objective function of RM shaper
g	Gravitational acceleration
j	Imaginary unit

l_1	Length between first and second joint of grapple
l_2	Length between second joint and center of mass of grapple
m	Mass of grapple
n	Number of impulses
q_1	Slewing angle
q_1, x, z	Cylindrical position of tip
r	Reference
s	Laplace variable
t	Time
t_i	Time location of impulse i
u	System input
x	State of system
x_m, y_m, z_m	Cartesian position of tip
y	Measured output

1. INTRODUCTION

In forest industry, forest as a working environment causes safety and productivity challenges due to working in various and difficult terrains and weather conditions. With automation and robotics, the productivity and safety of the workforce has been increased in different fields of industry. Safety and productivity improvements are also possible in forest industry with advances in automation and robotics. [1]

Furthermore, fluent operation of forestry machine requires plenty of training which has introduced an interest towards partially or fully automated motions [2]. For an inexperienced operator, smooth operation of the forestry crane is difficult task and joystick-based control might lead to oscillations in hydraulic actuators, crane structure and unwanted swaying motion of the grapple [3].

In construction sites, factories and harbours, boom cranes are widely used to move heavy payloads. In boom cranes, fast motion commands lead to payload swaying problems and slow settling, which make unloading difficult. Moreover, the swaying motion of the payload decreases productivity, efficiency and safety. [4] Similar problems can be found in forestry crane operation. With fast motion commands from the operator, the grapple starts swaying which makes the operation of the boom more difficult. Also, a grapple that sways excessively poses a higher safety risk.

In cut-to-length system, machines are generally divided into harvesters and forwarders. The machine types differs from each other by the purpose they are used for. Whereas harvesters are used to fell and process the trees, forwarder is picking up the the felled trees and transporting them to predefined location. [2]

1.1 Control of cranes with freely hanging load

With hydraulic forestry crane, control strategies for sway reduction of grapple or tool is not widely researched topic [5]. In [5], nonlinear model predictive control was implemented and tested for sway reduction with forestry crane that has freely hanging tool attached to its tip. In objective function, control effort, difference between measured and reference tip position and velocity, tool swaying and extension length were minimized. With nonlinear model predictive control, the sway angles of the tool was reduced by 64% in perpendicular

direction and by 76 % in parallel direction. [5]

In [3], input shaping technique to attenuate swaying motion of the payload induced from inner boom actuator was tested with laboratory down-sized forwarder crane. More specifically, zero vibration input shaper was applied to valve currents to reduce the swaying motion. The sway of the payload was not directly measured or observed and instead the oscillations in torque of the inner boom joint, calculated from measured pressure, were observed. However, significant reduction in the amplitude of oscillations in torque was noticed. [3]

In [6], automated slewing motion of forestry crane was implemented while considering the attenuation of the swaying of freely hanging grapple. Torque measurement of slewing was used in generation of optimal trajectories for slewing angular position. With smooth preplanned trajectories and feedback position control of angular position of slewing movement, reduction in swaying motion was discovered. [6]

In addition to forestry cranes, overhead cranes are commonly used in factories to move heavy objects. In overhead crane, trolley can be moved horizontally in two perpendicular directions. The hanging load is attached with cable to trolley and can sway to both of the movement directions. [7]

With overhead cranes, control strategy to achieve minimal residual vibration in minimal control time has been investigated for long time [8]. Residual vibration has been attenuated with different open-loop methods that includes feedforward with notch [9],[10] and low-pass filters [11] and input shaping [8].

In [8], modified input shaping control is studied to limit the sway angle of the payload during movement and when end point is reached. Difference of the proposed and regular input shapers is how the sway angle during movement is taken into account. As in regular input shaper, only the residual vibration is considered, the proposed modified input shaper also presents a constraint that restricts the sway angle during movement to be below certain value. This constraint is added to optimization problem from which the pulse amplitudes and time locations of the pulses are solved for input shaper. With simulation results, it was found that the modified input shaper is more effective in reduction of sway angle during movement but as a downfall, the movement time of the payload was increased. [8]

In addition, an infinite impulse response (IIR) Butterworth low-pass filter with different orders are studied with laboratory size overhead crane system [11]. The low-pass filters are design to have cut-off frequency at 50% of the first mode of sway to extract input energy around the natural frequencies. With 3^{rd}, 6^{th} and 9^{th} order low-pass filters, it was concluded that higher order filter provides more reduction of swaying motion. However, the response becomes slower when the order of the filter is increased. [11]

From filtering techniques, notch filter can be also used to extract the input energy around the natural frequencies. With notch filters, one filter for every natural frequency is required to extract the input energy. Individual notch filters are designed to have center cut-off frequencies at natural frequencies of the system. [11] The notch filter is studied to provide reduction in swaying motion with water tank load [9] and cubic load [10].

Rotary cranes are close to forestry cranes what comes to the mechanical structure. they can be divided in two groups, boom cranes and tower cranes. The difference between the crane types lies on how the load cable attachment point can be moved. Also, other degrees of freedom includes the rotation of crane structure and hoisting and lowering of the payload. [7]

With boom cranes, for example, model predictive control [12] and command shaping techniques [4] have been studied to reduce swaying motion of the payload. Also, command shaping technique has also been studied with tower cranes [13] and in addition, studies has covered gain scheduling [14] and delayed position [15] feedback control methods for reduction of swaying motion.

With both crane types, it was concluded that the load swaying motion was successfully suppressed with input shaping [4], [13]. However, it was noticed with tower cranes that input shaping causes a long lag to commands of operator [13]. This issue has been tried to solve with reduced-modification (RM) input shaper where the main idea is to modify the command signal as little as possible without swaying motion of load [16]. Also, different type of input shapers were studied with different cranes. Instead of regular input shaper, three impulse zero-vibration-derivation (ZVD) [4] and extrainsensitive (EI) [13] shapers were studied to provide more robustness.

With boom cranes, also low-pass and band-stop filters were compared with input shaping. Reduction in swaying motion was observed even with erroneous natural frequencies with all three methods. However, it was concluded that input shaping provides the biggest improvement to sway reduction when error in the natural frequency occurred. According to this observation, input shaping is more robust method towards variation in natural frequency. It was also noted that low-pass filter performs better than band-stop filter when used as input filter. [4]

For open-loop sway control, also optimal trajectory planning is studied with rotary cranes. To obtain suppression of swaying motion, combination of polynomial and cycloidal functions was observed to be effective. It was also stated that the proposed method is relatively simple but still effective to anti-sway control of tower crane. [17]

For hydraulic crane with hanging payload, control method to attenuate payload swaying in parallel direction compared to crane structure has been proposed. The control method utilizes kinematic functions for enabling control of the payload angle in parallel with po-

sition and velocity feedforward controllers. The controller is then tested with simulation and laboratory experiments. In both cases, the payload swaying motion is successfully suppressed. [18]

From closed-loop methods, model predictive control (MPC) has been proven to be applicable for combined anti-sway and reference tracking control of boom crane. In the studied case, MPC method decides the control action based on reference tracking and sway reduction terms. The performance of the MPC is then tested with commercial boom crane and stated as a potential control method for simultaneous reference tracking and sway reduction. [12].

With tower crane, gain-scheduled state feedback control with payload mass and rope length as scheduling parameters is studied for combined position and sway angle control. The controller was designed to perform a point-to-point movement of payload without large swaying motion. The gain-scheduled state feedback controller was validated with simulations and experimental setup to reduce the load swaying movement when simultaneously moving the payload. [14]

Delayed position feedback control is also studied matter in sway reduction with human operated tower crane. The proposed controller uses inherent time delays of the system by selecting proper gain and delay combination. The research also states an advantage compared to velocity feedback control. The same amount of damping is achievable with smaller gain when using delayed position feedback control. The results of the study shows a significant reduction in the swaying motion of the payload both in simulations and in experiments. [15]

1.2 Methods, research questions and thesis structure

In this thesis, an input shaping technique for reducing the swaying motion of the grapple is proposed. Input shaping is an open-loop control technique that has several drawbacks compared to closed-loop control. Firstly, closed-loop control systems are robust to uncertainties and parameter changes when properly designed. Secondly, closed-loop control systems are capable of regulating the controlled output to its desired value despite external disturbances. Thirdly, closed-loop control systems are able to change the output towards new desired values when set point is changed. However, closed-loop control has some drawbacks compared to open-loop control. For example, it can cause instability or oscillatory behaviour and increase the complexity of the system. They can also be sensitive to measurement noise. Open-loop control, however, is generally easy to design, and in most cases, the drawbacks of closed-loop control can be neglected. [19]

Input shaping is a control technique that can be used to reduce vibration in oscillatory systems such as cranes and other flexible structures. For preventing the excitation of

the oscillatory modes, input shaping technique used in this thesis requires estimates of natural frequency and damping ratio. That is, oscillatory modes are modelled using characteristics of second-order systems, and the reference input is modified such that residual vibrations are attenuated to zero. Input shaper modifies the command signal by delaying parts of the command signal such that the vibration caused by the first part of the signal is cancelled with the remaining parts. [20] In this thesis, the proposed control method is tested with a real forest machine.

The goal of this thesis is to use input shaping to prevent swaying motion of grapple. In [3], zero-vibration input shaper was tested with forestry crane to effectively damp oscillations induced from lifting cylinder movements. However, only lifting cylinder pressure was measured and comparison was made based on it. This approach does not directly address the reduction in grapple swaying, and therefore in this thesis, the swaying of grapple is directly measured during tests. Furthermore, the study showed reduction only in the pressure oscillations of lifting cylinder, with no observed improvement in the swaying of grapple. In this thesis, the swaying of grapple is directly prevented using reduced modification input shaper, presented in [16].

This thesis aims to answer the following research questions.

- To what extend can the grapple swaying be reduced with input shaping?
- How does changes in grapple orientation affect dampening ability of input shaping?
- How does parameter uncertainty of grapple affect the performance of input shaping?

The research questions have been formulated considering that a permanent sensor, which is capable of measuring the swaying motion, is unavailable in a real machine. However in this thesis, swaying of grapple has to be measured for identification and validation purposes, and thus, a temporary sensor is attached to the physical grapple. The input shaping compensator, however, is designed without measured information of the grapple swaying.

The material in this thesis is organised in six chapters. Chapters 2 and 3 address general concepts of modelling and control and the context of the research. In Chapter 4, the model of grapple is presented and studied, and the proposed control method explained. In the following Chapter 5, the testing procedure is discussed and the results from the tests are shown. Finally, the thesis is concluded in Chapter 6.

2. FUNDAMENTALS OF MODELLING AND CONTROL

In general, control systems can be divided into open-loop and closed-loop control systems. The main difference between the two structures is the existence of feedback loop. Control actions of closed-loop systems are usually based on actuating error

$$e(t) = r(t) - y(t) \tag{2.1}$$

where r is the reference and y is measured output. This is also called negative or 1DOF (one-degree-of-freedom) error feedback system, where the control action is determined based on control error e. In open-loop control system, control action is determined in predefined way without feedback. [21] In figure 2.1, block diagrams of the open-loop and closed-loop control systems are presented.

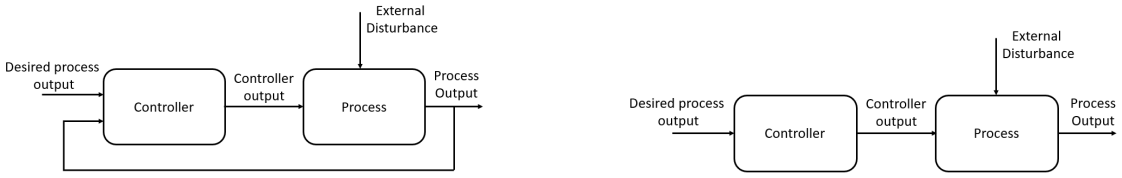

***(a)** Closed-loop control system* ***(b)** Open-loop control system*

***Figure 2.1.** Block diagrams of closed and open-loop control systems (Modified from [22])*

In control system design, it is essential to have a dynamic model in terms of knowledge of the system characteristics. The system model represents dynamics of the system in mathematical form, and it can be used to analyze the behaviour of the system and to design a controller for it. In any modelling process, a compromise has to be made between the accuracy and simplicity of the model. When dealing with system properties that has generally minor effect to system behavior, the simplifications are reasonable. Usually, it is desired to make a simple and low-order model of the system to begin with, and more precise model can be then obtained if necessary. [21]

2.1 Classification of dynamic systems

In [19], a model of a system is described to be "a mathematical representation of a physical, biological or information system". With the model, it is possible to study behaviour of

the system and to make prediction how the system will behave in specified circumstances. The model of the system is not unambiguous and the same system can be presented in multiple ways. The chosen model depends on the aspects of the system that are in scope of interest and what questions are tried to answer with the model. [19]

A system can be classified according to its nature. Number of inputs and outputs classifies the system into either single-input single-output (SISO), multi-input multi-output (MIMO), multi-input and single-output (MISO) or single-input multi-ouput (SIMO) systems. Also, classification into linear and non-linear systems can be made according to the principle of additivity

$$y(u_1 + u_2) = y(u_1) + y(u_2) \tag{2.2}$$

and the principle of homogeneity

$$y(k \cdot u_1) = k \cdot y(u_1) \tag{2.3}$$

where u_1 and u_2 are inputs of the system, y is the output of the system and k is real-valued constant parameter. [22]

The two principles in equations 2.2 and 2.3 form the principle of superposition

$$y(k_1 \cdot u_1 + k_2 \cdot u_2) = k_1 \cdot y(u_1) + k_2 \cdot y(u_2). \tag{2.4}$$

The principle of superposition states that if two individual inputs are applied to the system, the output of the system is the sum of individual outputs to those individual inputs. If the system satisfies the principle of superposition, the system is said to be linear. [21]

In addition, time invariance is an important aspect when system is studied. In time invariant system, the properties of the system do not change over time. In other words, if input $u(t)$ is applied to the system at a specific time, it results into output $y(t)$. If the same input is applied at later time $u(t + a)$, the output of the system will be $y(t + a)$. If the system satisfies preconditions for both linearity and time invariance, the system is called linear time invariant (LTI) system [19].

LTI systems has a useful property in which an arbitary input causes a response that is fully characterized by the impulse response. LTI system's response to any input $u(t)$ is

$$y(t) = \int_0^t h(t - \tau)u(\tau)\, d\tau, \tag{2.5}$$

where h is the impulse response of the system. [19]

An important aspect, when studying control systems, is stability. An LTI system is bounded-input bounded-output (BIBO) stable if and only if its response to bounded input is also bounded. However, if the system response to bounded input is unbounded, the system

is called unstable. The characterization between stable and unstable systems is called absolute stability. If the system is stable, the degree of stability can be evaluated. This evaluation is called relative stability. [23] To study absolute and relative stability of system, there exists several methods that are discussed in subsection 2.3.

2.2 Common model types of dynamic systems

In control engineering, generally two practices exist when dynamic model of the system is constructed. On the one hand, the mathematical model of a system can be formulated with differential equations. This practice is possible when the physical characteristics of the system are well known and simple enough to be constructed in a form of differential equations. For example, in mechanical and electrical systems, this approach is usually possible. On the other hand, the physical characteristics might be too complex to be modelled with differential equations. An alternative approach uses some experimental ways to study system output to a known input, which is known as system identification. [24]

In [25], various methods for system identification from input and output data are explained. For example, the convolution integral of equation 2.5 can be used to identify an arbitrary response of LTI system from its impulse response. Also, if sinusoidal input

$$u(t) = A \cdot sin(\omega t) \tag{2.6}$$

is applied to the LTI system, then its stationary response is given by

$$y(t) = A \cdot R(\omega) \cdot sin(\omega t + \phi(\omega)). \tag{2.7}$$

In the equation 2.7, A is the amplitude and ω is the angular frequency of the sinusoidal wave and $R(\omega)$ and $\phi(\omega)$ corresponds to magnitude ratio of the sinusoidal components between output and input and to the input and output phase difference, respectively. [25] From the knowledge of $R(\omega)$ and $\phi(\omega)$, frequency response of the system can be presented graphically using a Bode plot [19]. The Bode plot of a system is discussed more precisely in subsection 2.3.

The presented identification methods can be classified as classical methods for system identification. For classical identification methods, the result of identification is generally frequency response of the system in graphical form. The downfall of these methods occurs when studied system is not SISO system and more complex methods, for example posteriori identification, needs to be used. [25]

If a time-invariant nonlinear input-output differential equation of the system can be found,

then it is usually expressed using the following set of first-order differential equations

$$\begin{aligned} \frac{d\mathbf{x}(t)}{dt} &= f(\mathbf{x}(t), \mathbf{u}(t)) \\ \mathbf{y}(t) &= h(\mathbf{x}(t), \mathbf{u}(t)), \end{aligned} \tag{2.8}$$

where $\mathbf{x} \in \mathbb{R}^n$ is vector consisting state variables, $\mathbf{u} \in \mathbb{R}^p$ is vector consisting control signals and $\mathbf{y} \in \mathbb{R}^q$ is vector consisting measured signals. The equation 2.8 is in general form where functions f and h can be linear or nonlinear mappings of the state and control variables to the output.

The state **x** of the dynamic system is the smallest number of state variables that determines the system behaviour for any given input. Advantage of state-space modelling is the freedom to select the state variables. However, it is usually beneficial and conventional to select state variables to be easily measurable. Also, the freedom to select the state variables determines that the selection of state for specific system is not unique but a choice of design of the control system. [24]

In the equation 2.8, the differential equation was presented in general form where the mapping can be linear or nonlinear. Analysis and design of dynamic systems is much simpler, if f and h are linear. In case where mapping functions are linear, the general form of differential equation can be turned into linear state-space form of

$$\begin{aligned} \dot{\mathbf{x}}(t) &= \mathbf{A}\mathbf{x}(t) + \mathbf{B}\mathbf{u}(t) \\ \mathbf{y}(t) &= \mathbf{C}\mathbf{x}(t) + \mathbf{D}\mathbf{u}(t) \end{aligned} \tag{2.9}$$

where $\mathbf{x} \in \mathbb{R}^n$, $\mathbf{u} \in \mathbb{R}^p$, $\mathbf{A} \in \mathbb{R}^{n \times n}$, $\mathbf{B} \in \mathbb{R}^{n \times p}$, $\mathbf{C} \in \mathbb{R}^{q \times n}$ and $\mathbf{D} \in \mathbb{R}^{q \times p}$ are constant matrices. The formed system is both linear and time-invariant and thus an LTI-system. [19]

The nonlinear equation of 2.8 can be converted into linear state-space system using linearization. The linearization procedure uses Taylor series to approximate the system near given operating point of $\overline{\mathbf{x}}$ and $\overline{\mathbf{u}}$. [21] If we consider an equilibrium point of $\mathbf{x} = \overline{\mathbf{x}}$ and $\mathbf{u} = \overline{\mathbf{u}}$ for a system of equation 2.8, we can define a new state variables to be

$$\begin{aligned} \delta\mathbf{x} &= \mathbf{x} - \overline{\mathbf{x}}, \\ \delta\mathbf{u} &= \mathbf{u} - \overline{\mathbf{u}}, \\ \delta\mathbf{y} &= \mathbf{y} - h(\overline{\mathbf{x}}, \overline{\mathbf{u}}). \end{aligned} \tag{2.10}$$

The new state variables represents the perturbations near the equilibrium point. When operating close to equilibrium point, the new state variables are close to zero. Thus, higher-order terms of Taylor series can be neglected and only the first-order term taken into account. [19]

With the new state variables, the nonlinear system in equation 2.8 can be linearized. The linear model is now

$$\begin{aligned} \delta\dot{\mathbf{x}}(t) &= \mathbf{A} \cdot \delta\mathbf{x}(t) + \mathbf{B} \cdot \delta\mathbf{u}(t), \\ \delta\mathbf{y}(t) &= \mathbf{C} \cdot \delta\mathbf{x}(t) + \mathbf{D} \cdot \delta\mathbf{u}(t), \end{aligned} \tag{2.11}$$

where

$$\mathbf{A} = \frac{\partial f(\overline{\mathbf{x}}, \overline{\mathbf{u}})}{\partial \mathbf{x}}, \mathbf{B} = \frac{\partial f(\overline{\mathbf{x}}, \overline{\mathbf{u}})}{\partial \mathbf{u}}, \mathbf{C} = \frac{\partial h(\overline{\mathbf{x}}, \overline{\mathbf{u}})}{\partial \mathbf{x}}, \mathbf{D} = \frac{\partial h(\overline{\mathbf{x}}, \overline{\mathbf{u}})}{\partial \mathbf{u}}. \tag{2.12}$$

As stated before, the formed linear model approximates the nonlinear model near the equilibrium point. If the system state is drifted far from the equilibrium, the linear model may become inaccurate. [19]

The studied system of equations in 2.9 or in 2.11 is an LTI MIMO-system. In MIMO-system, the response of one specific input to one specific output can be studied with transfer function. In general, a single transfer function element $G_n(s)$ is the relation between the Laplace transformations of one specific output $y_n(t)$ and one specific input $u_n(t)$ of MIMO-system

$$G_n(s) = \frac{Y_n(s)}{U_n(s)}. \tag{2.13}$$

To obtain the complete transfer function from a state space model, Laplace transform is applied to the linear state-space model matrices of equation 2.12. A unique transfer function $G(s)$ of the system is

$$G(s) = \mathbf{C}(s\mathbf{I} - A)^{-1}\mathbf{B} + \mathbf{D}, \tag{2.14}$$

where **I** is identity matrix with same size of **A**. [23]

Usually, the zeros and poles of the transfer function are an object of interest. As poles are defined as the roots of the denominator of transfer function $G_n(s)$ in equation 2.13, they corresponds to the eigenvalues of the matrix **A** in state space model if there are not pole-zero cancellations. Therefore, the poles and zeros of the system defines the intrinsic dynamics of system. Then again, zeros are obtained from the roots of the numerator of $G_n(s)$ with SISO systems. As poles depends only on the dynamic matrix **A**, zeros depends on all matrices **A**, **B**, **C** and **D** of the state space system. [19]

2.3 Dynamic behaviour of systems

Generally, it can be stated that the first step in system analysis is modeling. When a model is formed, the system performance can be analyzed with various different methods. [21] The methods can be generally divided into time domain and frequency domain methods. Whereas in the time domain analysis, the response of system is studied with respect to time, in frequency domain it is done with respect to frequency. [23]

The performance analysis can be also categorized by the state of system in which the analysis is made. Stable transient response is the part of system response before the steady-state or stationary state is reached. During transient response, output of system reflects the difference between initial state and steady-state of the system. Steady-state response is the system response after the transient response is decayed. The shape of transient response is only function of system dynamics, whereas the steady-state response also depends on the input quantity. For periodic inputs, such as sinusoidal input, stationary response is typically periodical, and for constant inputs, steady-state is also constant. This requires that system is stable. Also, steady-state response is affected by DC-gain (Direct Current) of the system which is also called zero frequency gain. DC-gain can be pointed out from the steady-state output and magnitude of the constant input. The total response of the system is sum of these two response components. [19], [24]

Before further analyzing the system behaviour, the stability of the system has to be addressed since some physical systems are unstable by their nature. However, it is essential that the final control system is stable. [23]

As stated in subsection 2.1, an LTI system is stable if its response to bounded input is bounded. The absolute stability can be studied from the poles or eigenvalues of the LTI system. Poles are obtained from the roots of denominator of a SISO transfer function whereas eigenvalues of the system are eigenvalues of the dynamics matrix **A**. For system to be stable, necessary and sufficient condition is that the poles or eigenvalues of the system have negative real parts. In other words, the poles have to be on the left-hand side of the imaginary axis. Special case occurs when simple poles are at the imaginary axis and the system is called marginally stable. In this case, the system response to bounded input is sustained oscillation if the input is not sinusoidal with frequency equal to the magnitude of the pole. If the pole located in the imaginary axis is not single pole but multiple pole occurs, the system is unstable. [19], [23]

There are many tools to examine the behaviour of the system. During the stability analysis, pole-zero map might have been used since it graphically presents the locations of poles that are on interest. The idea of pole-zero map is to plot poles and zeros of the system in complex plane. General practice is to mark a place of pole with a cross and a place of zero with a circle. From the locations of the poles and zeros, some characteristics of the system can be obtained. [19] In figure 2.2, example pole-zero map is presented.

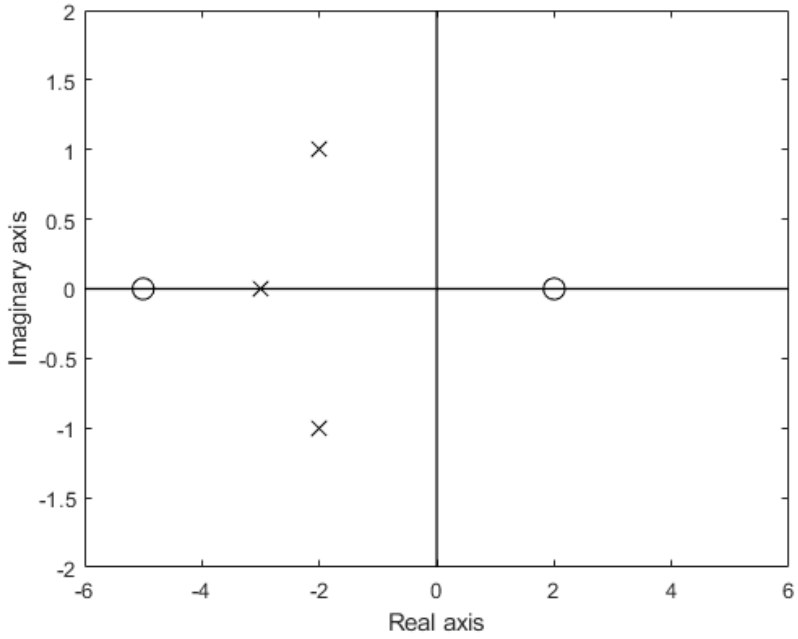

Figure 2.2. *Pole-zero map for example system with poles at -3 and $-2 \pm 1j$ and zeros at -5 and 2 (modified from [19])*

The locations of poles and zeros are easily seen in the pole-zero map. Especially from the location of the poles, some characteristics of the system including tendency to oscillate and speed of the response is easy to gather. Also, as stated before, stable system has poles only on the left hand side of the imaginary axis which can be easily confirmed from the pole-zero map. For stable poles, poles located on the real axis do not provoke oscillation to the response that poles with non-zero imaginary part does. Also, the distance from the real and imaginary axis gives some insight of the behaviour. The further the pole is from the imaginary axis, the faster the response is. Similarly, as the distance increases from the real axis, the frequency of the oscillation increases. Drawback of the pole-zero map is that the multiplicity of poles and zeros can not be deduced. Also, the DC-gain nor delay can not be determined from it. [23]

One way to study the system behaviour is from the frequency response point of view. Frequency response $G(j\omega)$ is attainable from the transfer function $G(s)$ by selecting the Laplace variable s from the positive imaginary axis. Frequency response gives knowledge how system behaves when the frequency of the input changes. As presented in equations 2.6 and 2.7, the frequency response of the system can be expressed with gain or magnitude $R(\omega)$ and phase $\phi(\omega)$ of the system. These are also obtainable from the frequency response $G(j\omega)$ of the system as follows: [19]

$$R(\omega) = |G(j\omega)| \tag{2.15}$$

$$\phi(\omega) = arg(H(j\omega)). \tag{2.16}$$

Frequency response is usually expressed in a form of Bode plot which consists of the magnitude and phase of the system plotted as a function of frequency on a logarithmic scale. In Bode plot, the gain of the system can be generally plotted in decibels and phase in degrees. The conversion from absolute gain to decibel gain can be done by taking base 10 logarithm of the absolute gain. [21]

$$R_{dB}(\omega) = 20log_{10}(|G(j\omega)|) \tag{2.17}$$

As an example, the Bode plot of

$$G(s) = \frac{1}{s^2 + 0.9s + 1} \tag{2.18}$$

is presented in figure 2.3, with $w = [0.1\ 100]$.

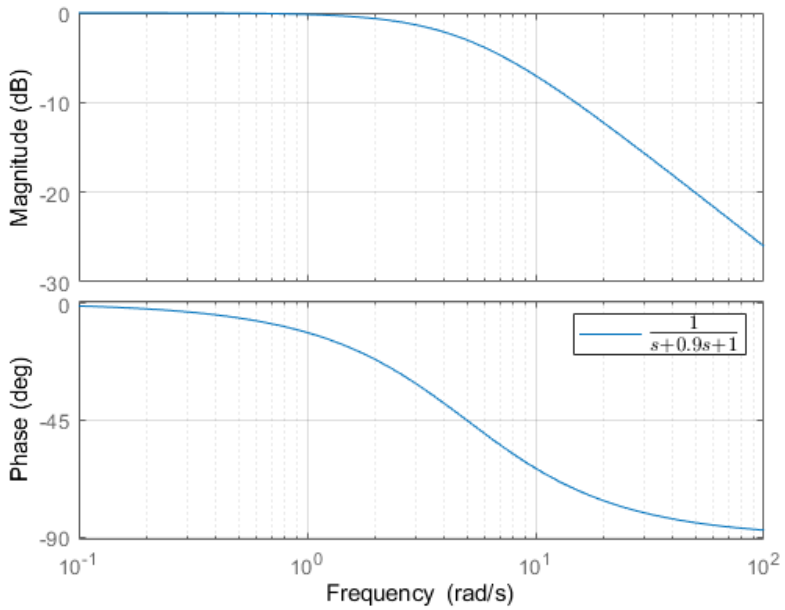

Figure 2.3. *Bode plot of an example system*

Generally, the Bode plot gives a quick overview of the dynamics of system. Usually, several different frequency ranges can be obtained from the bode plot. For example ranges where gain of the system is constant, decreasing and increasing are usually present. From these frequency ranges can be then said that amplitude of sinusoidal input signal on that specific frequency range remains constant, increases or decreases. [19]

From the amount of poles system has, some knowledge of the dynamic behaviour is gained. Categorization to first order, second order and higher order systems is made

from the knowledge of the amount of poles the system has. The first order and second order system models can be used to approximate also higher order systems. [21], [23]

The system characteristics can be studied based on the transfer function. At first, the main characteristics of a first order system is explained. The transfer functions of a stable first order system without delay and zero is

$$G(s) = \frac{K}{\tau s + 1}, \quad K \neq 0, \tau > 0 \tag{2.19}$$

where K is the DC-gain of the system and τ is the time constant. Time constant represents the time in which the systems response to step input has reached 63.2 $\%$ of the final value. Thus, in case of first order system, the system's reaction speed to change in the input is concluded from the time constant. Gain of the system, despite the order of the system, explains the steady-state behaviour of it. [21]

When the order of the system is two, the system in some cases have oscillatory behaviour that first order system is not capable of having. The general form of a stable second order system without delay and zero is

$$G(s) = \frac{K\omega_n^2}{s^2 + 2\xi\omega_n s + \omega_n^2}, \quad K \neq 0, \omega_n > 0, \xi \geq 0, \tag{2.20}$$

where K is the gain of the system, ξ is the damping ratio of system and ω_n is the natural frequency of the system. As for the first order system, time constant was the only parameter to describe the transient response of system. With second order system, natural frequency and damping ratio together defines the transient response. [23]

On one hand, damping ratio of second order system describes the tendency of system to oscillate. In table 2.1, guideline how damping ratio affect the step response of second order system is given. [21]

Table 2.1. *Effect of damping ratio to step response of second order system*

$0 < \xi < 1$	Underdamped	Complex pole pair $a \pm b\dot{j}$	Response has tendecy to oscillate
$\xi = 1$	Critically damped	Double pole on real axis	Fastest non-oscillatory response
$\xi > 1$	Overdamped	Two simple poles on real axis	Non-oscillatory response but slower than $\xi = 1$

On the other hand, natural frequency of the system describes the frequency in which the system oscillates if there is no damping. Therefore, in case where damping exists, damped natural frequency defines oscillation frequency in which the response tends to oscillate. The damped natural frequency can be calculated from the natural frequency and damping ratio as follows

$$\omega_d = \omega_n\sqrt{1 - \xi^2}, \quad \xi \in [0, 1], \tag{2.21}$$

where ω_d is the damped natural frequency. From the equation 2.21, it is noticeable that increase in damping ratio will reduce the damped natural frequency. [21]

The first and second order systems can be utilized when the system order is greater than two. In these cases, the first and second order transfer functions are used to model the higher order system. For example, third order system written with second and first order system is presented below. [21], [23]

$$G(s) = \frac{K_1 K_2 \omega_n^2}{(s^2 + 2\xi\omega_n s + \omega_n^2)(\tau s + 1)} = \frac{K_1 \omega_n^2}{(s^2 + 2\xi\omega_n s + \omega_n^2)} \cdot \frac{K_2}{\tau s + 1} \tag{2.22}$$

The response of the third order system in equation 2.22 can be then expressed from the responses of the second and first order systems [21]. The figure 2.4 presents the responses of first, second and third order systems to an unit step input.

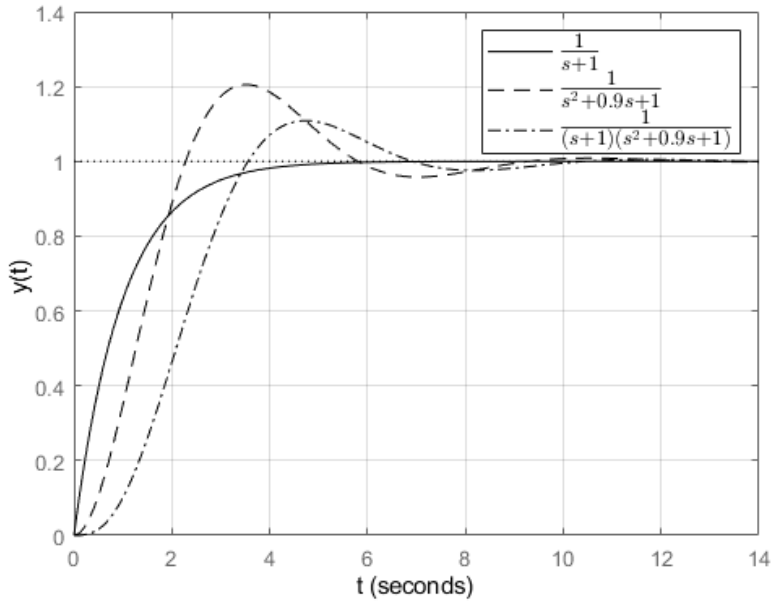

Figure 2.4. *Unit step responses of first, second and third order systems (modified from [21])*

Also, some roots of higher order system might affect the response more than the others. These roots are called dominant roots. In such case, where dominant roots exists, order of the system could be reduced by taking into account only the dynamics of dominating roots without excessively deteriorating the accuracy of the model. [19] The effect of dominating poles is presented in figure 2.5 where the dynamics of the second order pole pair is dominating over the first order pole.

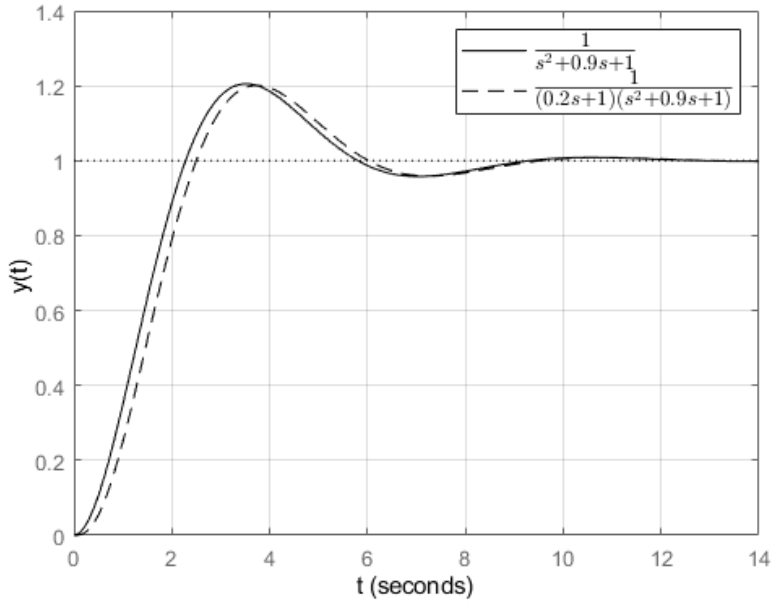

Figure 2.5. *Step responses of second and third order systems with dominant pole pair (modified from [21])*

The system models studied thus far have contained only poles. However, physical systems in some cases contains also zeros that are the roots of the numerator of the transfer function. As poles are defined directly from the properties of the system, some zeros depend on selection of inputs and outputs and how those are coupled to states. Because of this, those zeros of system can be affected by change of sensors and actuators or by introducing new ones. System can also have inherent zeros that can not be affected by feedback, but may be affected by compensators. [19]

The location of zero defines how much it affects the response of system. Generally, zero located closer to the dominant pole has more effect on the response than a zero that is located further away from it and also from the imaginary axis. This case is applicable when zero is located on the left hand side of the imaginary axis. [23]

If the zeros of the system are located on the right side of the imaginary axis, it is generally referred as a non-minimum phase system. These type of systems have their own difficulties when control is designed and such systems has some limitations in the performance that can be achieved. For a minimum phase system, that has no zeros on the right-hand side of imaginary axis and has no delay, the magnitude and phase-angle characteristics has unique relation. If magnitude curve of the system is specified, there exists a uniquely determined phase-angle curve. The unique relation works also other way around when the system has no delay and the sign of the DC-gain is known. However, this is not seen with non-minimum phase systems. The non-minimum phase zero also increases the phase lag of the system which decreases stability margins and causes the step response

to slow down. [21]

2.4 Feedforward control

Open-loop control system is presented in figure 2.1b where the two main components, controller and controlled process, are drawn in a form of block diagram. The purpose of the controller is to modify the command signal r that is desired process output and apply the modified command signal, called control signal u, to the process. The process output y will then in some accuracy follow the desired output. The drawback of the open-loop control is that the controller does not measure the process output and therefore is not capable of detecting changes in the process or its outputs. However, open-loop control is really simple control system to design. [26]

In general, closed-loop control is needed in systems where external disturbances exist. However, in some cases the output of the system is hard or impossible to measure or the effect of disturbances is small. In these cases, open-loop control might be a valid option. Also, open-loop control depends heavily on the knowledge of how the system behaves in certain conditions. Therefore, model of the system needs to be accurate enough to design proper open-loop controller. Open-loop controller is also easier to build from the point of view of stability. Such problems as over-correcting errors with closed-loop controller, does not exists with open-loop control. [21]

A proper combination of open-loop and closed-loop control is in many situations more cost effective and is capable of giving satisfying performance of system [21]. A way to combine open and closed-loop controllers is 2DOF (two-degree-of-freedom) control structure, where feedforward and feedback controllers are used [19]. The control method are emphasized in figure 2.6 in a block diagram form.

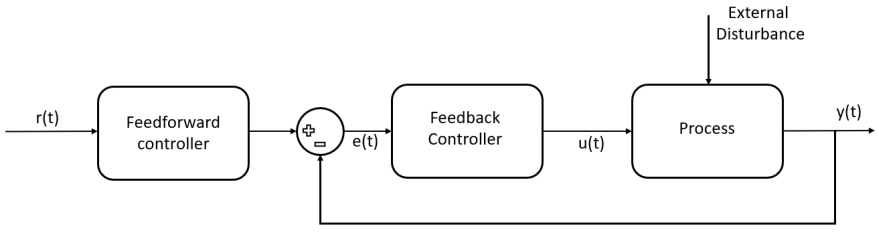

Figure 2.6. *Feedforward control system with feedback loop (modified from [19])*

In ideal conditions, where no disturbances and modelling error exists, feedforward controller is able to perform the control without the feedback loop. In these conditions, the control signal from those controllers has the desired response from the process and thus the error between desired output and measured output is zero. Therefore, the feedback loop is not needed. However, ideal conditions never exists and the purpose of feedback loop is to sense the difference in desired output and measured output caused by distur-

bances or inaccuracies in system model when feedforward controller is designed. [19]

Several ways to design the feedforward controller exist. The design depends on the main purpose of the controller that can be, for example purely control, as explained in previous paragraph or to cancel some unwanted behaviour from the system. For the second task, one way to approach it is to design the controller to cancel undesirable stable poles or zeros from the closed-loop system. Those might for example cause unwanted oscillation on the output of the system. Also, the controller in the closed-loop might not be able to affect these poles or zeros. This design method is generally stated as pole-zero cancellation. [26] For either of the cases, it is essential to be able to model the system [19].

2.5 Input shaping

In subsection 2.4, feedforward control was explained. Two different cases where the controller was used to purely control or on pole-zero cancellation were addressed. Input shaping could be included into pole-zero cancellation category since the main idea is to cancel oscillation from response which are due to stable complex conjugate pole pair. [27].

In a nutshell, input shaping is a control technique to reduce vibration in oscillatory system such as cranes and flexible structures. Technique uses the knowledge of system natural frequency and damping ratio to modify the input signal such that residual vibrations are attenuated to zero. Input shaper modifies the command signal by delaying parts of the command signal such that the vibration caused by the first part of the signal is cancelled with the remaining parts. [20] Figure 2.7 illustrates the input shaping process for impulse input where the initial command A is divided into two separate commands A_1 and A_2. Whereas individual commands A, A_1 and A_2 will have oscillatory responses, in total response of $A_1 + A_2$ oscillations are cancelled with the provoked oscillations of individual commands A_1 and A_2.

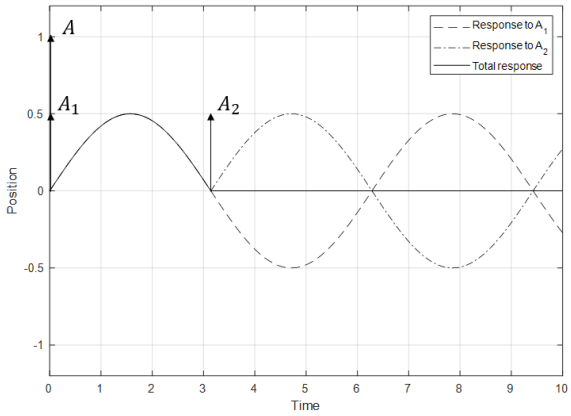

Figure 2.7. *Input shaped impulse response for arbitrary undamped oscillatory system (modified from [20])*

The main task in design of the input shaping algorithm is to determine the size of impulses A_i and times t_i when specific impulse is applied. Therefore, an optimization problem presented in equation 2.23 is constructed for given value of n. [20]

$$\begin{aligned} \underset{A_1,...,A_n,t_1,...,t_n}{min} \quad & t_n \\ s.t. \quad & \sum_{i=1}^{n} A_i = 1 \\ & t_{i+1} > t_i, i = 1, ..., n-1 \\ & V(\omega_n, \xi) = \frac{\omega_n}{\sqrt{1-\xi^2}} e^{-\xi\omega_n t_n} \sqrt{C(\omega_n,\xi)^2 + S(\omega_n,\xi)^2} = 0 \end{aligned} \tag{2.23}$$

In the optimization problem, the last constraint relates to the residual vibration $V(\omega, \xi)$, where [20]

$$\begin{aligned} C(\omega,\xi) &= \sum_{i=1}^{n} A_i e^{\xi\omega_n t_i} cos(\omega_n t_i \sqrt{1-\xi^2}) \\ S(\omega,\xi) &= \sum_{i=1}^{n} A_i e^{\xi\omega_n t_i} sin(\omega_n t_i \sqrt{1-\xi^2}). \end{aligned} \tag{2.24}$$

The residual vibration $V(\omega_n, \xi)$ expresses the percentage of the remaining residual vibration when the input shaping algorithm has been implemented. This assumption is valid when the natural frequency of the system ω_n and damping ratio ξ are precisely known. Therefore, in real life applications, the residual vibrations are always not exactly zero. The decreasing error between the modelled and actual natural frequencies will rapidly increase the residual vibration. One way to increase robustness is to increase the number of applied impulses. Also, more robust input shaping algorithms has been developed. The downfall of the increasing robustness is the increased time of the last applied impulse. [28]

The robustness of the input shaper can be increased by adding a robustness constraint to optimization problem in 2.23 given by

$$\frac{\partial V(\omega, \xi)}{\partial \omega} = 0. \tag{2.25}$$

In the presented constraint, the derivative of residual vibration is forced to zero at modelling frequencies. With robustness constraint, the shape of sensitivity curve can be affected and more robust behaviour near the modelling frequency gained. Also, the sensitivity of the input shaper can be adjusted by not setting the residual vibration to be zero but allow it in certain acceptable level. [29]

As mentioned, the input shaping technique actually cancels the oscillatory poles of the system with a corresponding zeros. The derivative constraint in equation 2.25 adds a second zero exactly at the same place with the oscillatory pole which sets the higher-order derivatives to zero [30]. Also, more robustness has been achieved by not setting the pole exactly on the same place with the pole but in the neighbourhood. The downfall of the additional robustness is the decrease in response time. However, if the system model is not accurate and error in the modelled natural frequency occurs, the decrease of the response time relative to attenuation of oscillations is acceptable. [28]

The optimization problem in 2.23 is able to cancel oscillations resulting from one natural frequency. However, some systems have several natural frequencies and are called multi-mode systems. The easiest way to design an input shaping algorithm for such systems is to design independent input shaper for each mode of oscillation and combine the results in series. This means that both of the resulting input shapers are used to filter the command signal which however, increases the number of impulses. [28] More efficient way is to add own residual vibration constraint $V(\omega_{ni}, \xi_i)$ for all modes to the design of same input shaper [31].

The discussion so far has only addressed the case where the input is in a form of impulse. However, in a real system such impulse shaped inputs are not generally used. One advantage of input shaping is that even if the basic design considered only impulse input, it can be used with any desired command to gain zero residual vibrations. Since the input sequence does not cause any residual vibration, the convolution product of the original sequence with desired command has the same property. [28]

3. GRAPPLE MODELLING, INSTRUMENTATION AND CONTROL METHODS

As discussed in chapter 2, the essential part of the control design is to know basic characteristics of the system. To gain the needed knowledge, system model is created. The model is then used to study the system behaviour.

In case of forest machine grapple, the modelling is based on the mechanical structure of it. Thus, differential equations to model and predict the behaviour of grapple can be constructed. The differential equations are then studied and input shaping algorithm designed based on the characteristics of the system.

3.1 Dynamic model of grapple

The basic structure, in addition to the grapple, includes link and rotation motor. Further on, the construction of these three parts is referred simply as grapple. Grapple is presented in figure 3.1.

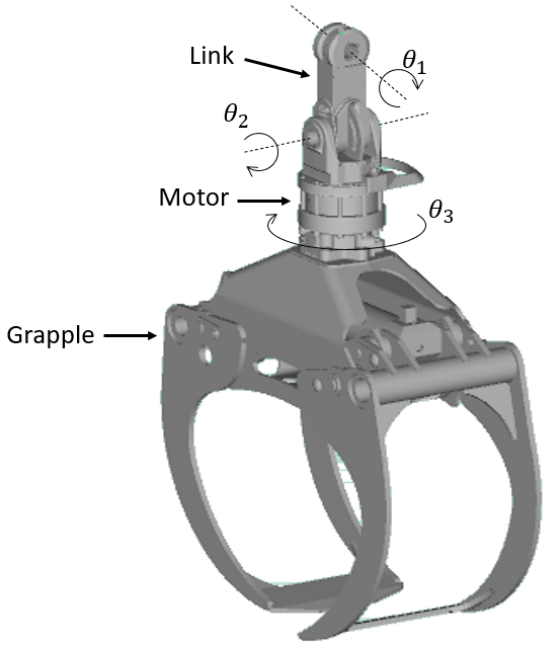

Figure 3.1. *Illustration of the forest machine grapple*

The grapple has three joints θ_1, θ_2 and θ_3 around which it can rotate. The link has two free joints θ_1 and θ_2 in both ends where the upper joint connects the whole grapple to the tip of the crane as seen in figure 3.1. The rotation around these two joints is free and can not be directly controlled. The third joint θ_3 however, is controllable by hydraulic motor and with it, the grapple orientation respect to the crane can be changed. Also, the grapple can be opened and closed with two hydraulic cylinders inside the grapple.

The grapple can be simplified for modelling purpose. The main assumption in [32] is that all mass of grapple is located at one point in end of two link parts. This will exclude the rotational inertia from the dynamic equations but will simplify the model significantly. However, the angular velocities of the grapple are low and thus, the rotational inertia is neglected. [32] In the figure 3.2, the simplified grapple is illustrated.

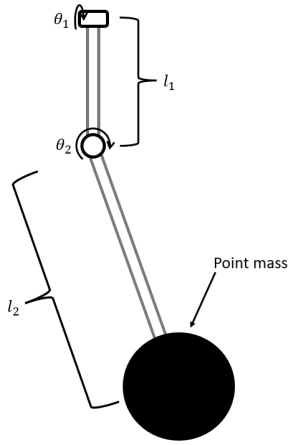

Figure 3.2. *Simplified grapple with its mass modelled as point mass*

In the figure 3.2, l_1 is the length between the first and second joint and l_2 is the length from second joint to the center of mass of the grapple part. At this point, the third rotational degree of freedom θ_3 is not point of interest since the swaying motion happens in the freely rotating joints. However, how the orientation of grapple affects the swaying motion will be studied during the testing procedure.

For the simplified grapple, Langrangian formulation can be applied to derive the dynamical model of the system. Lagrangrian is "energy-based" approach to dynamics where the torque of each joint in the system is

$$\tau_i = \frac{d}{dt}\frac{\partial L}{\partial \dot{\omega}_i} - \frac{\partial L}{\partial \omega_i} \tag{3.1}$$

where L is the difference between kinetic T and potential V energy called Lagrangian. [32], [33]

$$L = T - V \tag{3.2}$$

The equation 3.1 states that the Lagrangian and thus the kinetic and potential energy has

to be modelled for the torque equations of the joints. In [32], the equation of kinetic and potential energy are formed for the simplified grapple and joint torques τ_{θ_1} and τ_{θ_2} are derived as follows:

$$\begin{aligned}\tau_{\theta_1} =& ml_3(l_3\ddot{\theta}_1 + cos(\theta_1)\ddot{y}_m + sin(\theta_1)(\ddot{z}_m + g) \\ & - 2l_2 sin(\theta_2)\dot{\theta}_1\dot{\theta}_2 - l_2 cos(\theta_1)sin(\theta_2)\ddot{q_1} \\ & - l_3 sin(\theta_1)cos(\theta_1)\dot{q_1}^2 - 2l_2 cos(\theta_1)cos(\theta_2)\dot{\theta}_2\dot{q_1})\end{aligned} \tag{3.3}$$

$$\begin{aligned}\tau_{\theta_2} =& ml_2(l_2\ddot{\theta}_2 - cos(\theta_2)\ddot{x}_m - sin(\theta_1)sin(\theta_2)\ddot{y}_m \\ & + cos(\theta_1)sin(\theta_2)(\ddot{z}_m + g) + l_3 sin(\theta_2)\dot{\theta}_1^2 \\ & + sin(\theta_1)(l_1 cos(\theta_2) + l_2)\ddot{q_1} + sin(\theta_2)(l_1 - l_3 cos^2(\theta_1))\dot{q_1}^2 \\ & + 2l_3 cos(\theta_1)cos(\theta_2)\dot{\theta}_1\dot{q_1}).\end{aligned} \tag{3.4}$$

In the equations 3.3 and 3.4, $l_3 = l_1 + l_2 cos(\theta_2)$, $\ddot{x}_m$, $\ddot{y}_m$ and $\ddot{z}_m$ are the accelerations of the tip of the crane in base coordinate system, q_1 is the slewing angle, m is mass of grapple and g is gravitational acceleration. In the figure 3.3, moving joints and base coordinate system of the crane is expressed.

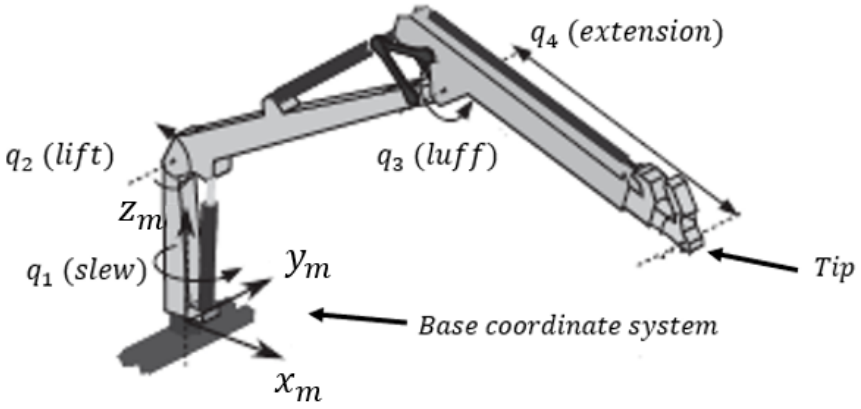

Figure 3.3. *Joints and base coordinate system of the crane (modified from [5])*

Swaying of the grapple is damped due to existing friction in the joints. In the equations 3.3 and 3.4, torques τ_{θ_1} and τ_{θ_2} are thus modelled as viscous friction:

$$\begin{aligned}\tau_{\theta 1} &= -b_{\theta 1}\dot{\theta}_1 \\ \tau_{\theta 2} &= -b_{\theta 2}\dot{\theta}_2.\end{aligned} \tag{3.5}$$

In equation 3.5, the torque caused by the friction is linearly dependant of the friction coefficient $b_{\theta n}$ and the angular velocity of the joint $\dot{\theta}_n$. [34] There exists several more precise methods to model friction as the presented one. The advantage of the viscous friction model is that only one parameter has to be identified for single joint. In this case,

the simplicity of the model is prioritized over the preciseness. [32]

The dynamic model of sway angles of the grapple can be now formed by substituting the friction equations 3.5 to the torque equation of the joints 3.3 and 3.4.

$$\begin{aligned}\ddot{\theta}_1 =& f_1(\theta_1, \theta_2, \dot{\theta}_1, \dot{\theta}_2, \dot{q}_1, \ddot{q}_1, \ddot{x}_m, \ddot{y}_m, \ddot{z}_m) \\ =& \frac{1}{l_3}(-cos(\theta_1)\ddot{y}_m - sin(\theta_1)(\ddot{z}_m + g) \\ & + 2l_2 sin(\theta_2)\dot{\theta}_1\dot{\theta}_2 + l_2 cos(\theta_1)sin(\theta_2)\ddot{q}_1 \\ & + l_3 sin(\theta_1)cos(\theta_1)\dot{q_1}^2 + 2l_2 cos(\theta_1)cos(\theta_2)\dot{\theta}_2\dot{q}_1 - \frac{b_1}{l_3 m}\dot{\theta}_1)\end{aligned} \tag{3.6}$$

$$\begin{aligned}\ddot{\theta}_2 =& f_2(\theta_1, \theta_2, \dot{\theta}_1, \dot{\theta}_2, \dot{q}_1, \ddot{q}_1, \ddot{x}_m, \ddot{y}_m, \ddot{z}_m) \\ =& \frac{1}{l_2}(cos(\theta_2)\ddot{x}_m + sin(\theta_1)sin(\theta_2)\ddot{y}_m \\ & - cos(\theta_1)sin(\theta_2)(\ddot{z}_m + g) - l_3 sin(\theta_2)\dot{\theta}_1^2 \\ & - sin(\theta_1)(l_1 cos(\theta_2) + l_2)\ddot{q}_1 - sin(\theta_2)(l_1 - l_3 cos^2(\theta_1))\dot{q_1}^2 \\ & - 2l_3 cos(\theta_1)cos(\theta_2)\dot{\theta}_1\dot{q}_1 - \frac{b_2}{l_2 m}\dot{\theta}_2)\end{aligned} \tag{3.7}$$

The formed equations are nonlinear and linearization is needed. Also, accelerations $\ddot{x}_m$, $\ddot{y}_m$ and $\ddot{z}_m$ are expressed in cartesian base coordinate system (x_m,y_m,z_m) (see figure 3.3) whereas crane is operated in cylindrical coordinate system (q_1,x,z) presented in figure 3.4.

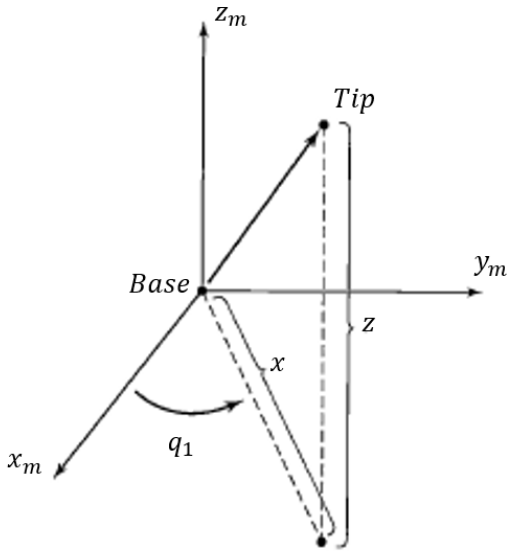

Figure 3.4. *Crane tip position in cylindrical coordinate system (modified from [33])*

Accelerations in cartesian coordinate system can be expressed in cylindrical coordinates as follows [5]:

$$\begin{aligned}\ddot{x}_m &= -sin(q_1)(\ddot{x} - x\dot{q}_1^2) - cos(q_1)(x\ddot{q}_1 + 2\dot{x}\dot{q}_1)\\ \ddot{y}_m &= -cos(q_1)(\ddot{x} - x\dot{q}_1^2) + sin(q_1)(x\ddot{q}_1 + 2\dot{x}\dot{q}_1)\\ \ddot{z}_m &= \ddot{z}.\end{aligned} \tag{3.8}$$

Now the dynamical model of grapple is expressed in cylindrical coordinate system by substituting equation 3.8 into dynamical model of the system in equations 3.6 and 3.7. To have an LTI state-space model for the grapple, the dynamical equations has to be linearized by utilizing the Taylor series presented in subsection 2.2. The linear differential equations are presented in 3.9.

$$\begin{aligned}\ddot{\theta}_1 =& a_1\theta_1 + a_2\theta_2 + a_3\dot{\theta}_1 + a_4\dot{\theta}_2 + a_5q_1 + a_6\dot{q}_1 + a_7\ddot{q}_1 + a_8x + a_9\dot{x} + a_{10}\ddot{x} + a_{11}\dot{z} + a_{12}\ddot{z}\\ \ddot{\theta}_2 =& b_1\theta_1 + b_2\theta_2 + b_3\dot{\theta}_1 + b_4\dot{\theta}_2 + b_5q_1 + b_6\dot{q}_1 + b_7\ddot{q}_1 + b_8x + b_9\dot{x} + b_{10}\ddot{x} + b_{11}\dot{z} + b_{12}\ddot{z}\end{aligned} \tag{3.9}$$

Equation 3.9 presents the linear model of grapple where

$$\begin{aligned}a_1 = \frac{\partial\bar{f}_1}{\partial\theta_1},\ a_2 = \frac{\partial\bar{f}_1}{\partial\theta_2},\ a_3 = \frac{\partial\bar{f}_1}{\partial\dot{\theta}_1},\ a_4 = \frac{\partial\bar{f}_1}{\partial\dot{\theta}_2},\ a_5 = \frac{\partial\bar{f}_1}{\partial q_1},\ a_6 = \frac{\partial\bar{f}_1}{\partial\dot{q}_1},\\ a_7 = \frac{\partial\bar{f}_1}{\partial\ddot{q}_1},\ a_8 = \frac{\partial\bar{f}_1}{\partial x},\ a_9 = \frac{\partial\bar{f}_1}{\partial\dot{x}},\ a_{10} = \frac{\partial\bar{f}_1}{\partial\ddot{x}},\ a_{11} = \frac{\partial\bar{f}_1}{\partial\dot{z}},\ a_{12} = \frac{\partial\bar{f}_1}{\partial\ddot{z}}\end{aligned} \tag{3.10}$$

and

$$\begin{aligned}b_1 = \frac{\partial\bar{f}_2}{\partial\theta_1},\ b_2 = \frac{\partial\bar{f}_2}{\partial\theta_2},\ b_3 = \frac{\partial\bar{f}_2}{\partial\dot{\theta}_1},\ b_4 = \frac{\partial\bar{f}_2}{\partial\dot{\theta}_2},\ b_5 = \frac{\partial\bar{f}_2}{\partial q_1},\ b_6 = \frac{\partial\bar{f}_2}{\partial\dot{q}_1},\\ b_7 = \frac{\partial\bar{f}_2}{\partial\ddot{q}_1},\ b_8 = \frac{\partial\bar{f}_2}{\partial x},\ b_9 = \frac{\partial\bar{f}_2}{\partial\dot{x}},\ b_{10} = \frac{\partial\bar{f}_2}{\partial\ddot{x}},\ b_{11} = \frac{\partial\bar{f}_2}{\partial\dot{z}},\ b_{12} = \frac{\partial\bar{f}_2}{\partial\ddot{z}},\end{aligned} \tag{3.11}$$

where $\bar{f}_1$ and $\bar{f}_2$ are f_1 and f_2 with equilibrium values. The crane is controlled with velocity commands ($\dot{q}_1$,$\dot{x}$,$\dot{z}$) in the cylindrical coordinate system which is also the input of the system $\mathbf{u} = [\dot{q}_1 \quad \dot{x} \quad \dot{z}]^T$. However, also the accelerations of the inputs exists in the linear equation in 3.9. By proper selection of the state vector **x**, the input derivatives are removed from the state space model. In 3.12, the states are presented.

$$
\begin{aligned}
x_1 =& \theta_1 \\
x_2 =& \theta_2 \\
x_3 =& \dot{\theta}_1 - a_7\dot{q}_1 - a_{10}\dot{x} - a_{12}\dot{z} \\
x_4 =& \dot{\theta}_2 - b_7\dot{q}_1 - b_{10}\dot{x} - b_{12}\dot{z} \\
x_5 =& q \\
x_6 =& x
\end{aligned}
\tag{3.12}
$$

To be able to form state space model, equations for first derivatives of states are needed. At first, the states in equation 3.12 are differentiated:

$$
\begin{aligned}
\dot{x}_1 =& \dot{\theta}_1 \\
\dot{x}_2 =& \dot{\theta}_2 \\
\dot{x}_3 =& \ddot{\theta}_1 - a_7\ddot{q}_1 - a_{10}\ddot{x} - a_{12}\ddot{z} \\
\dot{x}_4 =& \ddot{\theta}_2 - b_7\ddot{q}_1 - b_{10}\ddot{x} - b_{12}\ddot{z} \\
\dot{x}_5 =& \dot{q} \\
\dot{x}_6 =& \dot{x}.
\end{aligned}
\tag{3.13}
$$

Now, the first order derivatives of the states can be expressed with other state variables and system inputs by combining equations 3.9, 3.12 and 3.13.

$$
\begin{aligned}
\dot{x}_1 =& x_3 + a_7u_1 + a_{10}u_2 + a_{12}u_3 \\
\dot{x}_2 =& x_4 + b_7u_1 + b_{10}u_2 + b_{12}u_3 \\
\dot{x}_3 =& a_1x_1 + a_2x_2 + a_3x_3 + a_4x_4 + a_5x_5 + a_8x_6 \\
& (a_3a_7 + a_4b_7 + a_6)u_1 + (a_3a_{10} + a_4b_{10} + a_9)u_2 + (a_3a_{12} + a_4b_{12} + a_{11})u_3 \\
\dot{x}_4 =& b_1x_1 + b_2x_2 + b_3x_3 + b_4x_4 + b_5x_5 + b_8x_6 \\
& (b_3a_7 + b_4b_7 + b_6)u_1 + (b_3a_{10} + b_4b_{10} + b_9)u_2 + (b_3a_{12} + b_4b_{12} + b_{11})u_3 \\
\dot{x}_5 =& u_1 \\
\dot{x}_6 =& u_2
\end{aligned}
\tag{3.14}
$$

Finally, the state space model of the grapple is

$$
\begin{aligned}
\dot{\mathbf{x}} =& \mathbf{Ax} + \mathbf{Bu} \\
\mathbf{y} =& \mathbf{Cx} + \mathbf{Du},
\end{aligned}
\tag{3.15}
$$

where state and input vectors of the system are

$$\mathbf{x} = \begin{bmatrix} x_1 \\ x_2 \\ x_3 \\ x_4 \\ x_5 \\ x_6 \end{bmatrix} \quad \text{and} \quad \mathbf{u} = \begin{bmatrix} u_1 \\ u_2 \\ u_3 \end{bmatrix}, \tag{3.16}$$

and state space model matrices are

$$\mathbf{A} = \begin{bmatrix} 0 & 0 & 1 & 0 & 0 & 0 \\ 0 & 0 & 0 & 1 & 0 & 0 \\ a_1 & a_2 & a_3 & a_4 & a_5 & a_8 \\ b_1 & b_2 & b_3 & b_4 & b_5 & b_8 \\ 0 & 0 & 0 & 0 & 0 & 0 \\ 0 & 0 & 0 & 0 & 0 & 0 \end{bmatrix},$$

$$\mathbf{B} = \begin{bmatrix} a_7 & a_{10} & a_{12} \\ b_7 & b_{10} & b_{12} \\ a_3a_7 + a_4b_7 + a_6 & a_3a_{10} + a_4b_{10} + a_9 & a_3a_{12} + a_4b_{12} + a_{11} \\ b_3a_7 + b_4b_7 + b_6 & b_3a_{10} + b_4b_{10} + b_9 & b_3a_{12} + b_4b_{12} + b_{11} \\ 1 & 0 & 0 \\ 0 & 1 & 0 \end{bmatrix}, \tag{3.17}$$

$$\mathbf{C} = \begin{bmatrix} 0 & 0 & 1 & 0 & 0 & 0 \\ 0 & 0 & 0 & 1 & 0 & 0 \end{bmatrix} \quad \text{and} \quad \mathbf{D} = \begin{bmatrix} a_7 & a_{10} & a_{12} \\ b_7 & b_{10} & b_{12} \end{bmatrix}.$$

The angular velocities of grapple joints are selected as outputs of the system. The reasoning behind the selection will be further discussed in subsection 3.2. From the state space model in 3.17, transfer function matrix can be obtained using 2.14. The uncertain parameters l_1, l_2, b_1, b_2 and m are kept symbolic for further analysis of their effect to system parameters. Transfer function matrix is

$$G(s) = \begin{bmatrix} 0 & \frac{\frac{1}{l_1+l_2}s^2}{s^2+\frac{b_1}{m(l_1+l_2)^2}s+\frac{g}{l_1+l_2}} & 0 \\ \frac{-\frac{3}{l_2}s^2}{s^2+\frac{b_2}{ml_2^2}s+\frac{g}{l_2}} & 0 & 0 \end{bmatrix}. \tag{3.18}$$

From the transfer function matrix in 3.18, symbolic expression for natural frequency and damping ratio in both swaying directions are as follows:

$$\begin{aligned} \omega_{n_1} &= \sqrt{\frac{g}{l_1 + l_2}} \quad \text{and} \quad \xi_1 = \frac{b_1}{2m\sqrt{g}\sqrt{l_1 + l_2}^3} \\ \omega_{n_2} &= \sqrt{\frac{g}{l_2}} \quad \text{and} \quad \xi_2 = \frac{b_2}{2m\sqrt{g}\sqrt{l_2}^3}. \end{aligned} \tag{3.19}$$

In 3.19, ω_{n_1} and ω_{n_2} denote natural frequencies and ξ_1 and ξ_2 damping ratios of parallel and perpendicular swaying, respectively. Natural frequencies are depending only on system parameters l_1 and l_2, whereas b_1, b_2 and m affects also the damping ratio.

3.2 Measurement system for grapple swaying

To study grapple behaviour in real forest machine, a measurement system is needed. The measurement system attached to the real grapple is presented in figure 3.5.

Figure 3.5. *Measurement system attached to real grapple*

From figure 3.5 it can be seen that the measurement device is attached inside grapple and thus, will restrain testing with load. However, the measurement system is designed such that testing can be done with closed grapple. Also, it is noteworthy that attachment of measurement device is done with cable ties. Thus, calibration of measurement device is not precise and some variation in results might occur. Still, attachment is firm enough to provide useful measurement data for validation purposes. For identification, the proposed measurement device lack accuracy since it is not positioned exactly at the center of mass point of the grapple.

The measurement system consists of Intel RealSense t265 tracking camera, Raspberry

Pi 3B+ and powerbank. The tracking camera has two stereo cameras, IMU (Inertial Measurement Unit) and inbuilt SLAM (Simultaneous Localization And Mapping) algorithm to provide linear and angular position, velocity and acceleration data. When measurement is started, measurement system iniatializes world coordinate system to current location. All logged data is respect to that specific coordinate system. Figure 3.6 presents world coordinate frame (x, y, z) and measurement system coordinate frame (x', y', z') in case where swaying happens in parallel angle θ_1.

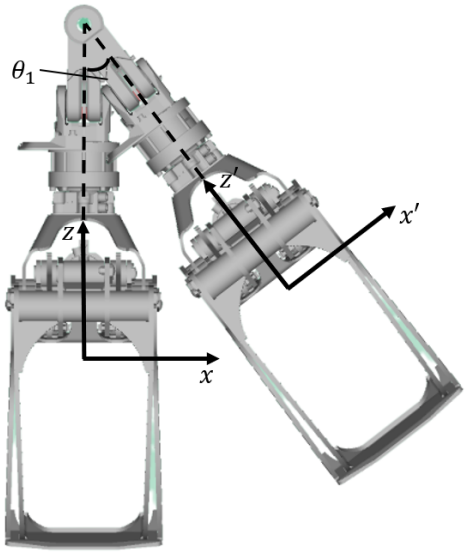

Figure 3.6. *Measurement system coordinate frames in parallel swaying* θ_1

From figure 3.6 it can be seen that when the world frame is attached to grapple in steady state, angular velocity of parallel swaying θ_1 is measured as rotation around y-axis. Similarly, angular velocity of perpendicular swaying is measured as rotation around x-axis. However, this requires that when grapple is in steady state, which means no swaying is detected, axes of world frame and measurement system coordinates frames has to be aligned. Therefore, world frame has to be rotated along crane.

Rotation along the crane means that world frame of measurement system has to be rotated along its z-axis. This can be done with a rotation matrix [33] given by

$$R(\theta) = \begin{bmatrix} cos(\theta) & -sin(\theta) & 0 \\ sin(\theta) & cos(\theta) & 0 \\ 0 & 0 & 1 \end{bmatrix}, \tag{3.20}$$

where θ is angle how much coordinate frame is rotated. As the world frame is wanted to rotate along the crane, following is gotten

$$\theta(t) = q_1(t) - q_1(0), \tag{3.21}$$

where q_1 is the slewing angle.

3.3 Experimental parameter identification of grapple

Nonlinear and linear models of grapple was formed in subsection 3.1. In this subsection, the nonlinear equation parameters are identified from real grapple measurement data. Furthermore, linear model is formed and characteristics of that studied. It is important to notice that identified parameters has uncertainty due to the measurement device.

First, measured data from the real grapple is collected. Data is collected from two cases where different inputs are applied to the system. In first case, tip velocity input $\dot{x}$ is applied. In second case, slewing angular velocity input q_1 is applied. The swaying angular velocities are measured in both cases. Figure 3.7 presents velocity command and measured velocities for both test cases.

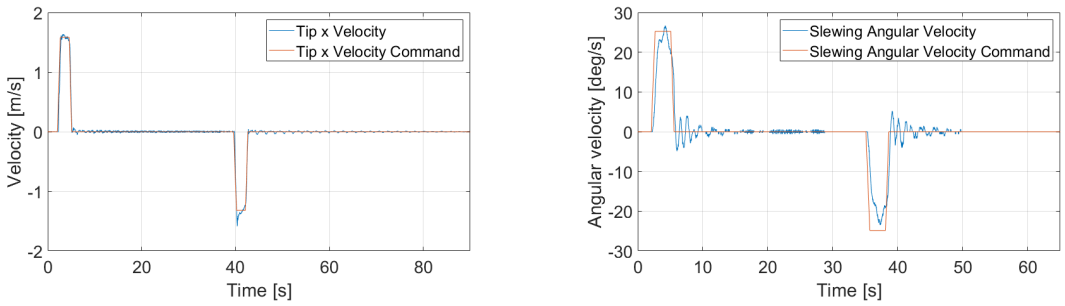

(a) *Tip x command* u_2 ***(b)*** *Slewing command* u_1

Figure 3.7. *Velocity command and measured velocity for two separate test cases*

In figures 3.8 and 3.9, measured swaying angular velocities for both test cases are presented.

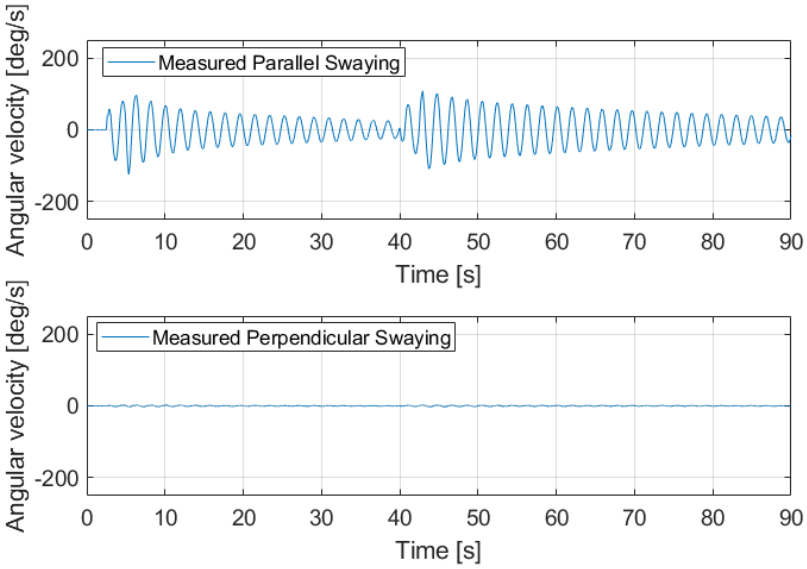

Figure 3.8. *Measured swaying velocities for tip x velocity input (u_2) in figure 3.7a*

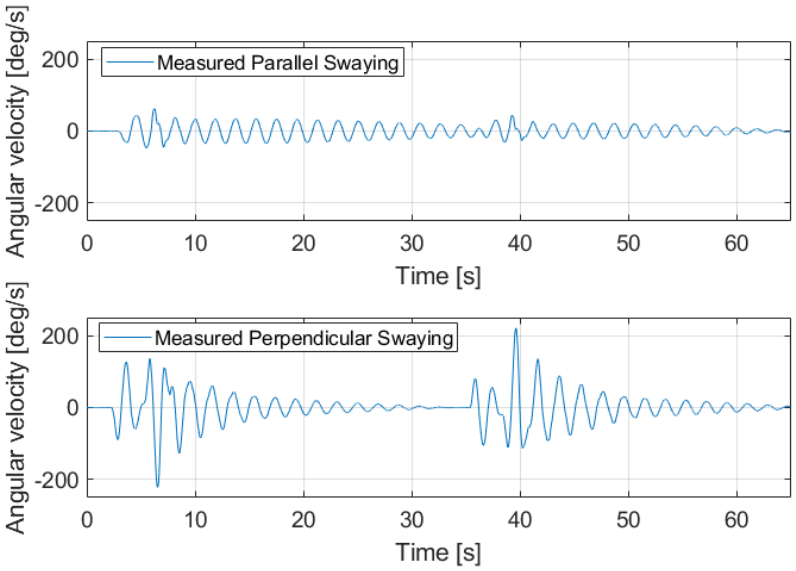

Figure 3.9. *Measured swaying velocities for slewing angular velocity input (u_1) in figure 3.7b*

Tunable parameters in the model equations 3.6 and 3.7 are viscous friction coefficients b_1 and b_2 which were tuned with measurement data and nonlinear simulation model of the grapple. The two lengths between joints are physical parameters of the grapple and thus should be constant. However in actual grapple, l_2 depends on the opening of the grapple. Opening and closing the grapple change the center of mass of the grapple. As l_2 denotes the length from lower joint to center of mass, this length change a little. The identification tests are done with partially open grapple seen in figure 3.1. All parameters of the model are collected to table 3.1.

Table 3.1. *Parameters of the nonlinear grapple model*

Length from first joint to second joint l_1	0.24 m
Length from second joint to center of mass of grapple l_2	0.66 m
Viscous friction coefficient of first joint b_1	45 $\frac{m \cdot kg}{s}$
Viscous friction coefficient of second joint b_2	55 $\frac{m \cdot kg}{s}$
Mass of grapple m	309.9 kg
Acceleration of gravity g	$9.81 \frac{m}{s^2}$

In figures 3.10 and 3.11, simulated angular velocities of swaying are compared with the measured data from real grapple.

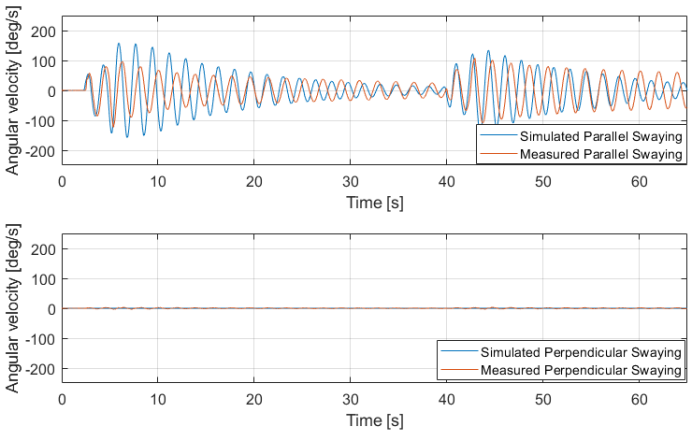

Figure 3.10. *Simulated and measured swaying angular velocities for tip x velocity input* (u_2) $(l_1 = 0.24m$ *and* $l_2 = 0.66m)$

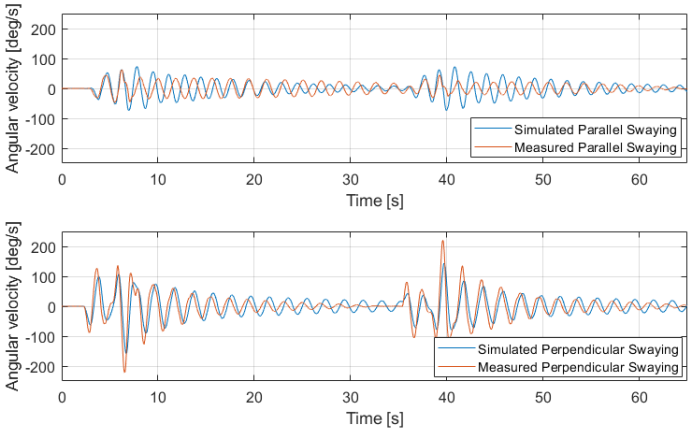

Figure 3.11. *Simulated and measured swaying angular velocities for slewing velocity input* (u_1) $(l_1 = 0.24m$ *and* $l_2 = 0.66m)$

In measured data, natural frequencies in both swaying directions are close to each other. However, the simulation model, based on model equations 3.6 and 3.7, gives natural frequencies that differs from each other. The main difference is detected in parallel direction.

Probable cause for this is that some physical aspect of the real grapple is not considered in the model. One of these aspects that probably affects the swaying is two hydraulic hoses attached to rotating motor of grapple. Figure 3.12 shows these two hoses.

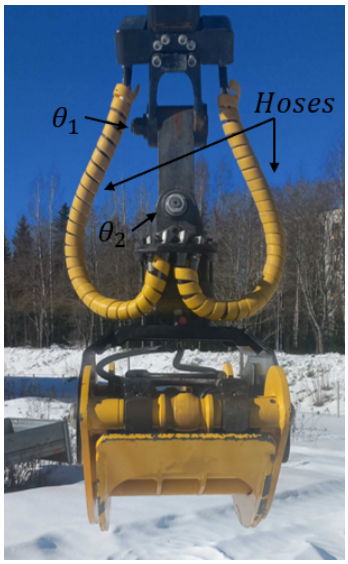

Figure 3.12. *Hoses that affect swaying in real grapple*

However, if $l_1 = 0m$ is selected, the model gives same natural frequency for both swaying directions. Table 3.2 collects natural frequencies from different cases where different values are tested. The friction coefficients are kept constant.

Table 3.2. *Experimental and simulated grapple swaying natural frequencies*

Natural frequency	Experimental	Simulated $l_1 = 0.24m, l_2 = 0.66m$	Simulated $l_1 = 0.05m, l_2 = 0.9m$
Parallel Swaying ($\frac{rad}{s}$)	3.26	3.77	3.29
Perpendicular Swaying ($\frac{rad}{s}$)	3.18	3.19	3.19

Selection $l_1 = 0.05m$ and $l_2 = 0.9m$ gives quite accurate natural frequency values from simulation model. Also, simulated swaying angular velocities are close to measured ones. Figures 3.13 and 3.14 presents these results.

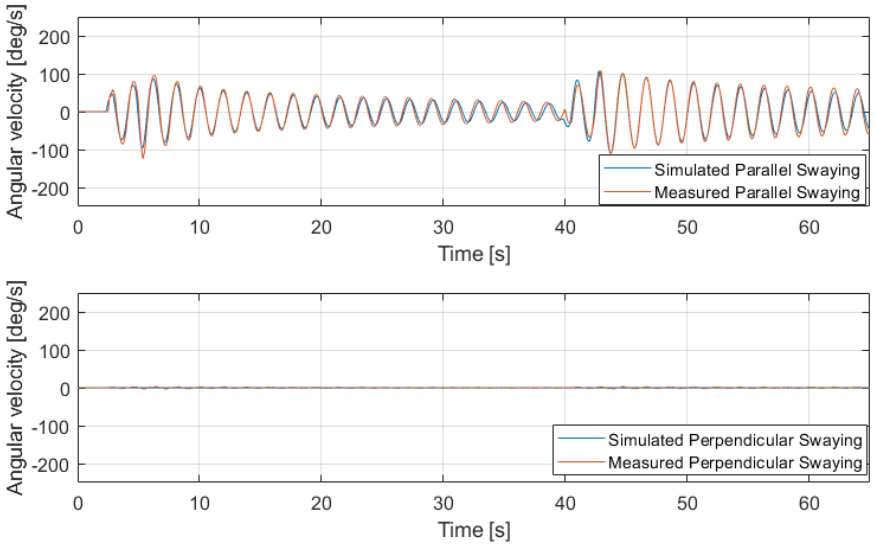

Figure 3.13. *Simulated and measured swaying angular velocities for tip x velocity input* (u_2) *(*$l_1 = 0.05m$ *and* $l_2 = 0.9m$*)*

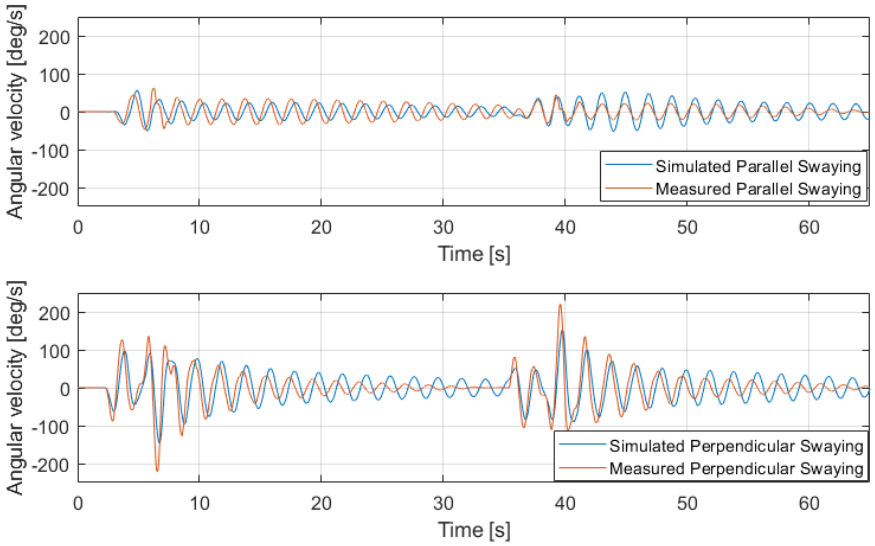

Figure 3.14. *Simulated and measured swaying angular velocities for slewing input* (u_1) *(*$l_1 = 0.05m$ *and* $l_2 = 0.9m$*)*

However, as mentioned in subsection 3.2, calibration of the measurement device causes some inaccuracies to results. Thus, the obtained results are indicative and can give an approximation how good the grapple model is. For more precise results, more accurate way to measure swaying has to be developed.

Improved model with tuned lengths l_1 and l_2 is used due to better simulation results. The linear grapple model using experimentally determined parameter values is

$$\dot{\mathbf{x}} = \begin{bmatrix} 0 & 0 & 1 & 0 & 0 & 0 \\ 0 & 0 & 0 & 1 & 0 & 0 \\ -10.33 & 0 & -0.1966 & 0 & 0 & 0 \\ 0 & -10.9 & 0 & -0.1793 & 0 & 0 \\ 0 & 0 & 0 & 0 & 0 & 0 \\ 0 & 0 & 0 & 0 & 0 & 0 \end{bmatrix} \mathbf{x} + \begin{bmatrix} 0 & 1.053 & 0 \\ -5.556 & 0 & 0 \\ 0 & -0.207 & 0 \\ 0.9959 & 0 & 0 \\ 1 & 0 & 0 \\ 0 & 1 & 0 \end{bmatrix} \mathbf{u}$$
$$\mathbf{y} = \begin{bmatrix} 0 & 0 & 1 & 0 & 0 & 0 \\ 0 & 0 & 0 & 1 & 0 & 0 \end{bmatrix} \mathbf{x} + \begin{bmatrix} 0 & 1.053 & 0 \\ -5.556 & 0 & 0 \end{bmatrix} \mathbf{u} \tag{3.22}$$

when the linearization point is chosen as

$$\begin{aligned} &\theta_1 = 0\, deg, \quad \theta_2 = 0\, deg, \quad \dot{\theta}_1 = 0\, \frac{deg}{s}, \quad \dot{\theta}_2 = 0\, \frac{deg}{s}, \quad q_1 = 0\, deg, \\ &\dot{q}_1 = 0\, \frac{deg}{s}, \quad \ddot{q}_1 = 0\, \frac{deg}{s^2}, \quad x = 5\, m, \quad \dot{x} = 0\, \frac{m}{s}, \quad \ddot{x} = 0\, \frac{m}{s^2}, \quad \dot{z} = 0\, \frac{m}{s}, \\ &\ddot{z} = 0\, \frac{m}{s^2} \end{aligned} \tag{3.23}$$

Matter of interest is dynamic characteristics of swaying. Thus, equation 3.18 can be utilized to form the transfer function matrix:

$$G(s) = \begin{bmatrix} 0 & \frac{1.053s^2}{s^2+0.1609s+10.33} & 0 \\ \frac{-3.33s^2}{s^2+0.2191s+10.9} & 0 & 0 \end{bmatrix}. \tag{3.24}$$

From the transfer function matrix, it can be noticed that according to linear model, the system is non-interacting and only tip x velocity input u_2 causes swaying in parallel direction and slewing velocity input u_1 in perpendicular direction.

From real grapple measurements in figures 3.8 and 3.9, it can be seen that actually slewing input u_1 causes swaying also in perpendicular direction. This is something that linear model approximation is not able to model. However, it is able to model the more significant swaying direction also in that case. The tip z velocity input u_3 is insignificant

from the viewpoint of swaying. Thus, zero transfer functions from that specific input to swaying angular velocities are justifiable.

The two nonzero transfer functions of the transfer function matrix are both second order transfer functions with two zeros as follows.

$$G_{u_1y_2} = \frac{-3.33s^2}{s^2 + 0.2191s + 10.9} \tag{3.25}$$

$$G_{u_2y_1} = \frac{1.053s^2}{s^2 + 0.1609s + 10.33} \tag{3.26}$$

At first, the stability of the system has to be addressed. For second order system, it adequate that all coefficients of the denominator polynomial have the same sign. As in 3.25 and 3.26, the coefficients are all positive, both of the systems are stable.

As stability has been studied, both of the transfer functions can be written into a form

$$G(s) = \frac{K\omega_n^2 s^2}{s^2 + 2\xi\omega_n s + \omega_n^2} \tag{3.27}$$

where ξ and ω_n denotes damping factor and natural frequency of second order system. Table 3.3 collects all parameters of equation 3.27.

Table 3.3. *Parameters of swaying transfer functions according equation 3.27*

	ξ	ω_n	K
$G_{u_1y_2}$	0.0332	3.302	-0.306
$G_{u_2y_1}$	0.0250	3.214	0.1019

Natural frequencies of the systems from linear model are thus 3.302 $\frac{rad}{s}$ for parallel direction and 3.214 $\frac{rad}{s}$ for perpendicular direction. These values are undamped natural frequency and thus, differ a little from the identified natural frequencies from the measured data. Damped natural frequency can be calculated with equation 2.21. Also noticeable is that swaying in both directions has a really low damping. System characteristics are also visible from frequency response of the system that are presented in figure 3.15.

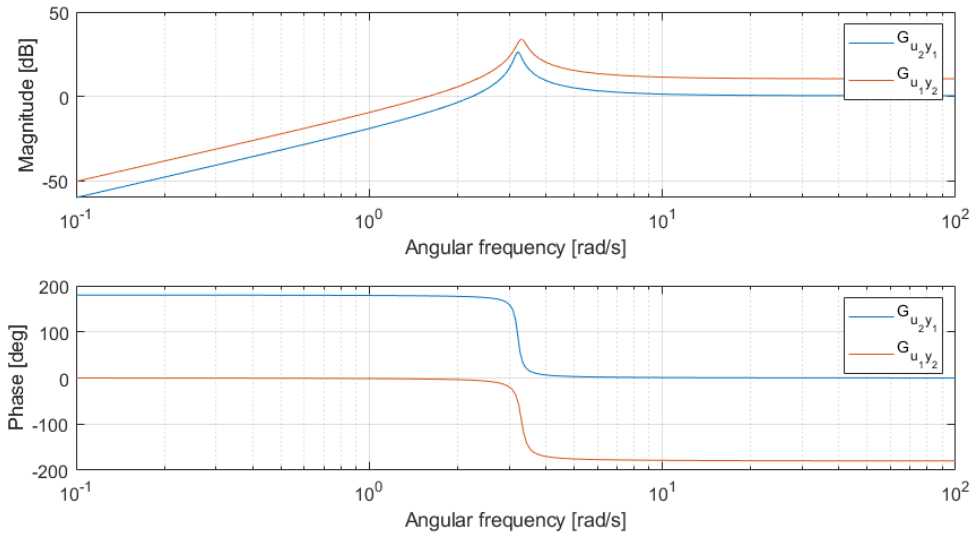

Figure 3.15. *Frequency response of grapple models*

Gains of both systems are really low for low frequency inputs and zero for zero frequency input because of the zero at the origin. Therefore, low frequency inputs do not affect as high swaying of grapple as high frequency inputs. This is relatively intuitive as really fast movement of crane will generate swaying with higher amplitude than slow movement. Also, DC-gain of the system is zero and thus, steady-state response of the system will eventually converge to zero. Intuitively, if the crane is stand still or moving on constant velocity, without external disturbances swaying of the grapple will eventually stop.

Highest gain for both systems exists at the natural frequency. For parallel direction peak gain is 26.5 dB at 3.21 $\frac{rad}{s}$ and for perpendicular 34.0 dB at 3.30 $\frac{rad}{s}$. Also, the parallel direction has slightly larger gain through whole frequency range. The Bode plot also emphasizes the swaying phase seen in 3.14. With slewing movement, parallel swaying has phase shift of 180 degrees compared to perpendicular swaying as seen also from Bode in 3.15.

3.4 Feedforward control of forestry crane with input shaping

Input shaping method was introduced in detail in subsection 2.5. In this subsection, a reduced modification (RM) shaper, presented in [16], is discussed for step input command. The main advantage of RM shaper is that the command is affected as little as possible while at the same time swaying is supressed. Introduced RM shaper will be later implemented and tested on the machine.

As mentioned in previous paragraph, RM shaper tries to minimize the difference between original and input shaped command. The error is thus denoted by $\epsilon(t)$. Therefore, objec-

tive function for RM shaper can be written as [16]

$$f = \int_0^\infty \epsilon(t)^2 dt. \tag{3.28}$$

The objective function is related to integral of squared error (ISE). The squaring ensures the positivity of the objective function. In input shaping optimization problem, amplitudes of impulses $A_1, ..., A_n$ and time locations $t_1, ..., t_n$ when each impulse is applied, are determined. Thus, the integral of the objective function in 3.28 can be simplified:

$$f = \int_0^\infty \epsilon(t)^2 dt = \sum_{i=1}^{n-1} (t_{i+1} - t_i)(1 - \sum_{j=1}^{i} A_j)^2. \tag{3.29}$$

This result is relatively easily understood from the graphical representation of original and input shaped commands presented in figure 3.16.

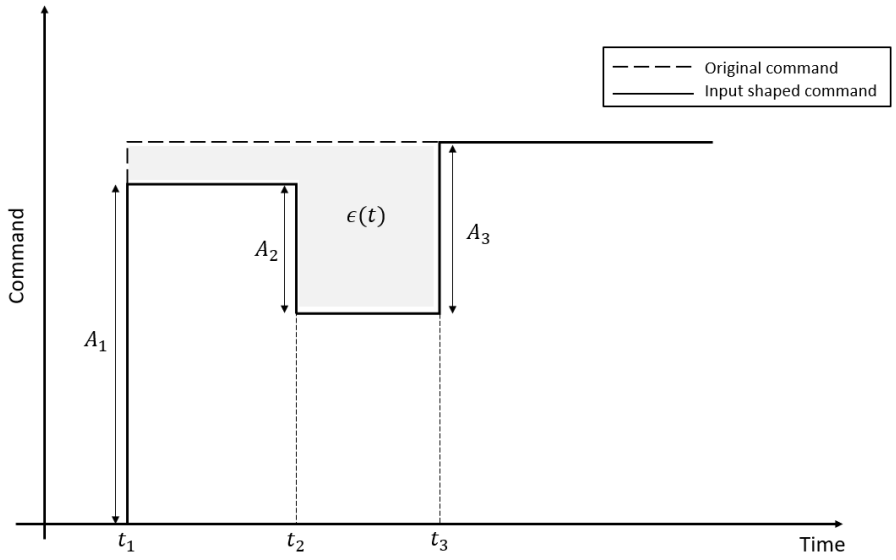

Figure 3.16. *Graphical presentation of error between original and input shaped command (modified from [16])*

In figure 3.16, command of three impulse input shaper is presented. The error between the two commands is marked as grey area. Now, the error can be divided into areas of two separate rectangles:

$$f = \int_0^\infty \epsilon(t)^2 dt = (t_2 - t_1)(1 - A_1)^2 + (t_3 - t_2)(1 - (A_1 + A_2))^2. \tag{3.30}$$

The objective function in equation 3.29 is now the generalized version of the objective function derived for three impulse case. Finally, the optimization problem, to determine amplitudes of impulses $A_1, ..., A_n$ and time locations $t_1, ..., t_n$ when each impulse is applied, is gotten by combining RM shaper objective function in equation 3.29 with the constraints of the regular input shaping problem of equation 3.31.

$$\begin{aligned} \underset{A_1,...,A_n,t_1,...,t_n}{min} \quad & \sum_{i=1}^{n-1}(t_{i+1}-t_i)(1-\sum_{j=1}^{i}A_j)^2 \\ s.t. \quad & \sum_{i=1}^{n}A_i = 1 \\ & t_{i+1} > t_i, i = 1, ..., n-1 \\ & V(\omega_n,\xi) = \frac{\omega_n}{\sqrt{1-\xi^2}} e^{-\xi\omega_n t_n}\sqrt{C(\omega_n,\xi)^2 + S(\omega_n,\xi)^2} <= V_{tol} \end{aligned} \tag{3.31}$$

The optimization problem is solved for both swaying directions individually for natural frequency and damping ratio presented in table 3.3. Table 3.4 presents the results for different pulse numbers n when $V_{tol} \approx 0$. For pulse numbers 3 and 5, also results, when 5% residual vibration ($V_{tol} <= 0.05$) is accepted, are presented. Value of objective is marked with f.

Table 3.4. *Results of RM shaper optimization problem*

	$G_{u_1y_2}$	$G_{u_2y_1}$
n = 2	A = [0.526 0.474] t = [0 0.98] f = 0.2202	A = [0.5211 0.4789] t = [0 0.95] f = 0.2179
n = 3	A = [0.8105 -0.3452 0.5347] t = [0 0.20 0.86] f = 0.1959	A = [0.8275 -0.3581 0.5306] t = [0 0.19 0.84] f = 0.1887
n = 4	A = [0.7739 -0.3415 0.2177 0.35] t = [0 0.23 0.70 0.89] f = 0.1864	A = [0.7057 -0.1966 -0.1217 0.6125] t = [0 0.25 0.55 0.82] f = 0.1953
n = 5	A = [0.8567 -0.2737 -0.162 0.2642 0.3149] t = [0 0.15 0.32 0.73 0.91] f = 0.1879	A = [0.835 -0.2798 -0.137 0.2604 0.3214] t = [0 0.17 0.34 0.70 0.89] f = 0.1797
n = 3 ($V_{tol} <= 0.05$)	A = [0.8378 -0.3391 0.5013] t = [0 0.19 0.86] f = 0.1879	A = [0.8361 -0.3425 0.5065] t = [0 0.18 0.83] f = 0.1797
n = 5 ($V_{tol} <= 0.05$)	A = [0.894 -0.2206 -0.2006 0.2537 0.2734] t = [0 0.13 0.27 0.75 0.91] f = 0.1618	A = [0.893 -0.2225 -0.2022 0.2554 0.2762] t = [0 0.12 0.26 0.73 0.89] f = 0.1617

Overall, the difference between results for different swaying direction is small. Only noticeable difference is that with four impulse shaper, third impulse is negative for parallel motion and positive for perpendicular. Also, the duration of RM shaper is between 0.8s and 1s in all cases. In general, value of objective function decreases when number of impulses increases.

To test a robustness of RM shaper, error in natural frequency and damping ratio was added to the optimization problem in 2.23. The applied error will depict a modelling error or variation and thus, test results will show how robust specific RM shaper is. Table 3.5 presents resulting RM shapers when $\pm 10\%$ error is applied to natural frequencies.

Table 3.5. *Results of RM shaper optimization problem with $\pm 10\%$ error in natural frequency*

$V_{tol} \approx 0$	$G_{u_1 y_2}$	$G_{u_2 y_1}$
n = 2 (+10% in ω)	A = [0.5176 0.4824] t = [0 0.89] f = 0.2071	A = [0.5167 0.4833] t = [0 0.86] f = 0.2009
n = 2 (-10% in ω)	A = [0.5212 0.4788] t = [0 1.09] f = 0.2499	A = [0.5212 0.4788] t = [0 1.06] f = 0.243
n = 4 (+10% in ω)	A = [0.7985 -0.3618 0.2556 0.3076] t = [0 0.20 0.67 0.84] f = 0.1734	A = [0.8173 -0.3721 0.2606 0.2943] t = [0 0.18 0.67 0.81] f = 0.1689
n = 4 (-10% in ω)	A = [0.8047 -0.3594 0.2532 0.3015] t = [0 0.25 0.83 1.03] f = 0.2062	A = [0.8246 -0.367 0.2597 0.2828] t = [0 0.22 0.83 0.99] f = 0.199
$V_{tol} <= 0.05$		
n = 3 (+10% in ω)	A = [0.8389 -0.3369 0.498] t = [0 0.17 0.78] f = 0.1557	A = [0.8361 -0.3425 0.5065] t = [0 0.17 0.76] f = 0.1559
n = 3 (-10% in ω)	A = [0.8381 -0.3385 0.5004] t = [0 0.21 0.96] f = 0.1933	A = [0.8379 -0.339 0.512] t = [0 0.21 0.93] f = 0.1863
n = 5 (+10% in ω)	A = [0.8922 -0.2242 -0.2035 0.2569 0.2785] t = [0.11 0.24 0.68 0.83] f = 0.1534	A = [0.8921 -0.2245 -0.2038 0.2572 0.279] t = [0 0.11 0.23 0.66 0.80] f = 0.1491
n = 5 (-10% in ω)	A = [0.8935 -0.2217 -0.2015 0.2547 0.275] t = [0 0.14 0.29 0.84 1.01] f = 0.1849	A = [0.8933 -0.222 -0.2018 0.255 0.2755] t = [0 0.14 0.29 0.81 0.99] f = 0.1778

As was obtained in 3.19, natural frequencies are only depending on l_1 and l_2 of the physical parameters of grapple. Therefore, the change needed in those parameters for such $\pm 10\%$ variation can be obtained as follows

$$\omega_{n_2} = \sqrt{\frac{g}{l_2}} \quad \Leftrightarrow \quad l_2 = \frac{g}{\omega_{n_2}^2} \tag{3.32}$$

whereas

$$0.9\omega_{n_2} = \sqrt{\frac{g}{l_2}} \quad \Leftrightarrow \quad l_2 = 1.234\frac{g}{\omega_{n_2}^2} \tag{3.33}$$

and thus, 23.4% increase in l_2 is needed for -10% variation in natural frequency. With ω_{n_1}, similar increase is needed for $l_1 + l_2$. For $+10\%$ variation, the change needed in l_2 or $l_1 + l_2$ is -17.4% which can be obtained by replacing 0.9 with 1.1 in 3.33. The increase and decrease would require change in the physical dimensions of the grapple as only l_2 can be minorly affected by adding a load to grapple. The load will thus change the location of the center of mass of the grapple and affect accordingly to l_2. However, with different grapple types, the presented changes of 23.4% and -17.4% are possible.

The effect of natural frequency to resulting RM shaper is clearly seen from table 3.5. Higher natural frequency results in longer lasting RM shaper as smaller natural frequency. However, size of impulses remains almost the same. Value of objective function increases

when natural frequency decreases. Also, the decrease in objective function value is seen when impulse number is increased. Second case is to add error to damping factor and have natural frequency at constant value. Resulting RM shapers, when damping ratio is increased to five times higher and smaller, is presented in table 3.6.

Table 3.6. *Results of RM shaper optimization problem with 5 times larger or smaller damping ratio*

$V_{tol} \approx 0$	$G_{u_1y_2}$	$G_{u_2y_1}$
n = 2 (5·ξ)	A = [0.6161 0.3839] t = [0 0.99] f = 0.1459	A = [0.6068 0.3932] t = [0 0.96] f = 0.1484
n = 2 ($\frac{1}{5}\cdot\xi$)	A = [0.5049 0.4951] t = [0 0.98] f = 0.2402	A = [0.506 0.494] t = [0 0.95] f = 0.2318
n = 4 (5·ξ)	A = [0.8611 -0.2969 0.2063 0.2295] t = [0 0.24 0.80 0.94] f = 0.1184	A = [0.8368 -0.2957 0.1994 0.2595] t = [0 0.25 0.74 0.92] f = 0.122
n = 4 ($\frac{1}{5}\cdot\xi$)	A = [0.8173 -0.3817 0.2701 0.2943] t = [0 0.20 0.76 0.92] f = 0.1989	A = [0.815 -0.3831 0.2711 0.297] t = [0 0.18 0.74 0.89] f = 0.2001
$V_{tol} <= 0.05$		
n = 3 (5 ·ξ)	A = [0.8763 -0.2636 0.3874] t = [0 0.22 0.89] f = 0.1039	A = [0.8709 -0.274 0.403] t = [0 0.21 0.86] f = 0.1091
n = 3 ($\frac{1}{5}\cdot\xi$)	A = [0.8314 -0.3517 0.5203] t = [0 0.18 0.86] f = 0.1892	A = [0.8313 -0.352 0.5207] t = [0 0.18 0.83] f = 0.1814
n = 5 (5 ·ξ)	A = [0.9195 -0.1703 -0.1584 0.2132 0.196] t = [0 0.15 0.30 0.80 0.95] f = 0.099	A = [0.8165 -0.2474 -0.0819 0.194 0.3189] t = [0 0.22 0.42 0.7 0.89] f = 0.1375
n = 5 ($\frac{1}{5}\cdot\xi$)	A = [0.8889 -0.2307 -0.209 0.2629 0.2878] t = [0 0.12 0.26 0.75 0.91] f = 0.1798	A = [0.9231 -0.1586 -0.153 -0.1415 0.5299] t = [0 0.08 0.16 0.25 0.82] f = 0.1786

As only l_1 and l_2 parameters affect natural frequencies of the grapple, also b_1, b_2 and m have effect on damping ratio. Damping ratio is directly proportional to damping coefficients b_1 and b_2 and inversely proportional to mass m. Increase in mass, for example log in the grapple, will decrease damping ratio proportionally. For effect of l_1 and l_2, following can be obtained

$$\xi_2 = \frac{b_2}{2m\sqrt{g}\sqrt{l_2}^3} \quad \Leftrightarrow \quad l_2 = (\frac{b_2}{2m\sqrt{g}\xi_2})^{\frac{2}{3}} \tag{3.34}$$

whereas

$$5\xi_2 = \frac{b_2}{2m\sqrt{g}\sqrt{l_2}^3} \quad \Leftrightarrow \quad l_2 = 2.92(\frac{b_2}{2m\sqrt{g}\xi_2})^{\frac{2}{3}} \tag{3.35}$$

and thus, for perpendicular swaying, l_2 has to be almost triple. Similarly, with five times smaller damping ratio, l_2 has to be only 34% of its original value. With parallel swaying, same reasoning is valid for sum $l_1 + l_2$. As discussed previously when error in natural frequency occurred, the possible way to achieve such high changes would require change

in a physical dimensions of the grapple. Thus, to achieve the presented change in damping ratio is physically meaningful by changing the damping coefficients or mass of the grapple. However, only increase of mass is possible by adding logs. As mass is inverse proportional to natural frequency, only five times smaller damping ratio can be achieved with five times higher mass of the grapple. With damping coefficients, such five times higher or smaller values could be possible and depends at least on the greasing of joints.

When damping ratio is changed, mainly magnitude of amplitudes of RM shaper change. However, also time locations when the amplitudes do change but the change is smaller as it was with error in natural frequency. Value of objective function is higher with smaller damping ratios. To conclude the effect of error in RM shapers, it can be said that location and size of amplitudes are connected to the model parameters. Also, the objective function value depends on those and in addition, the number of amplitudes affects it.

4. OBSERVATIONS AND RESULTS FROM MACHINE TESTING

4.1 Machine test scenarios for input shaping

Test scenarios for input shaping can be divided into two separate cases. In first scenario, slewing angular velocity command (u_1) presented in figure 3.7b is applied. In second scenario, similar velocity command is applied for tip x (u_2) direction that is presented in figure 3.7a. In both cases, a back-and-forth movement is done where positive and negative pulses are applied with proper settling time of swaying in between. The pulses are ramp up commands from zero to maximum velocity in specific direction and back to zero.

At first, it is noticed that measured slewing angular velocity tends to oscillate. This can be seen from figure 3.7a where especially when angular velocity is ramped to zero, the measured angular velocity oscillates around the zero. This movement causes some swaying of grapple on top of the actual pulse command. Similar behaviour was also detected with input shaping algorithm which can be seen in figure 4.1.

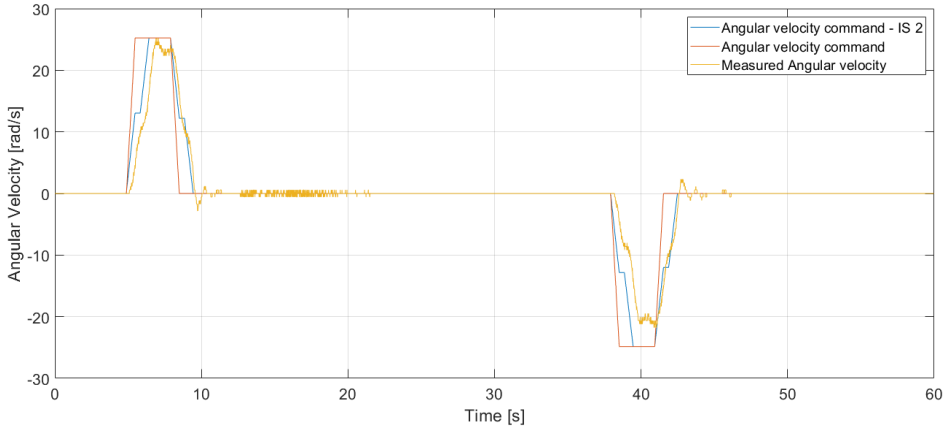

Figure 4.1. *Slewing test scenario with 2 impulse RM shaper*

How RM shaper modifies the ramp input is also presented in figure 4.1 in case where two impulse RM shaper is used. Even though there exists oscillations in the measured angular velocity, those are not as high as they was without RM shaper. However, they will

still affect the swaying of grapple. Other important aspect to notice from the figure 4.1 is that the resulting angular velocity of slewing is not able to follow the modified command well. This is more evident when RM shaper that has negative impulses are used. Figure 4.2 presents the result for 4 impulse RM shaper.

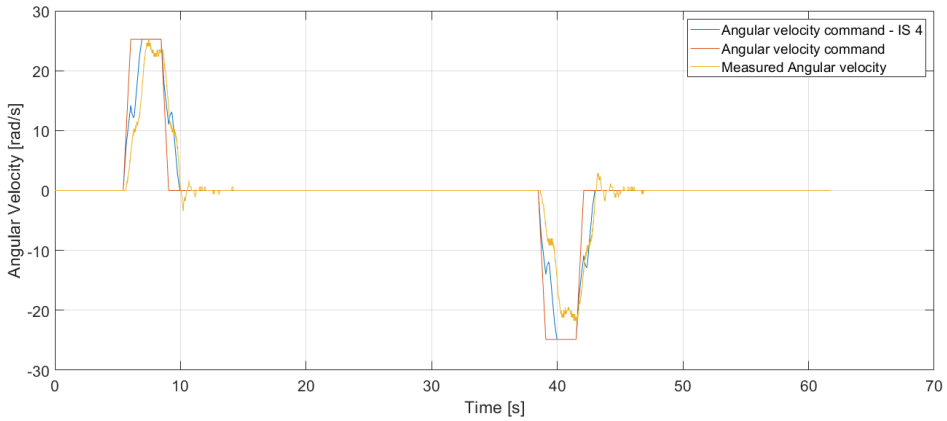

Figure 4.2. *Slewing test scenario with 4 impulse RM shaper*

Negative impulse in RM shaper causes a small deceleration period to command which the angular velocity is not able to follow. The capability of slewing to follow command is one important aspect to discuss when perfomance of RM shaper is discussed.

For tip x velocity command, similar behaviour is not noticed and command is followed relatively well. Figure 4.3 presents command and measured tip velocity when 4 impulse RM shaper is used.

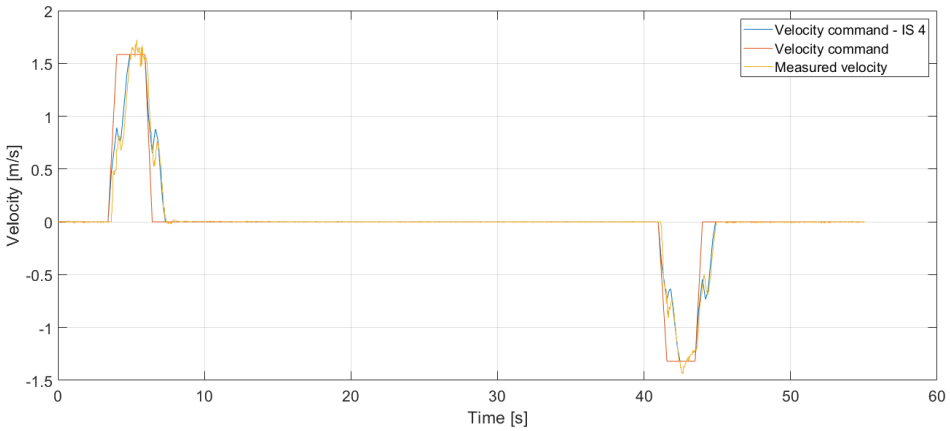

Figure 4.3. *Tip x test scenario with 4 impulse RM shaper*

Also, from figure 4.3 it can be seen that there are no oscillations in the velocity when the movement is stopped.

4.2 Effect of grapple orientation to swaying

Figure 3.1 shows that grapple has 3 degrees of freedom around which it can rotate. The third angle θ_3 is called rotation angle and is the only one that operator can control. In this subsection, the effect of rotation of grapple to swaying is studied. Basically, two different cases where grapple is orientated such that log in the grapple is parallel or perpendicular to crane is studied. In addition, the effect of grapple opening (closed or open) to natural frequency is studied.

First, the effect of grapple rotation in slewing test scenario is studied. Figure 4.4 presents swaying in both direction when the grapple is oriented differently.

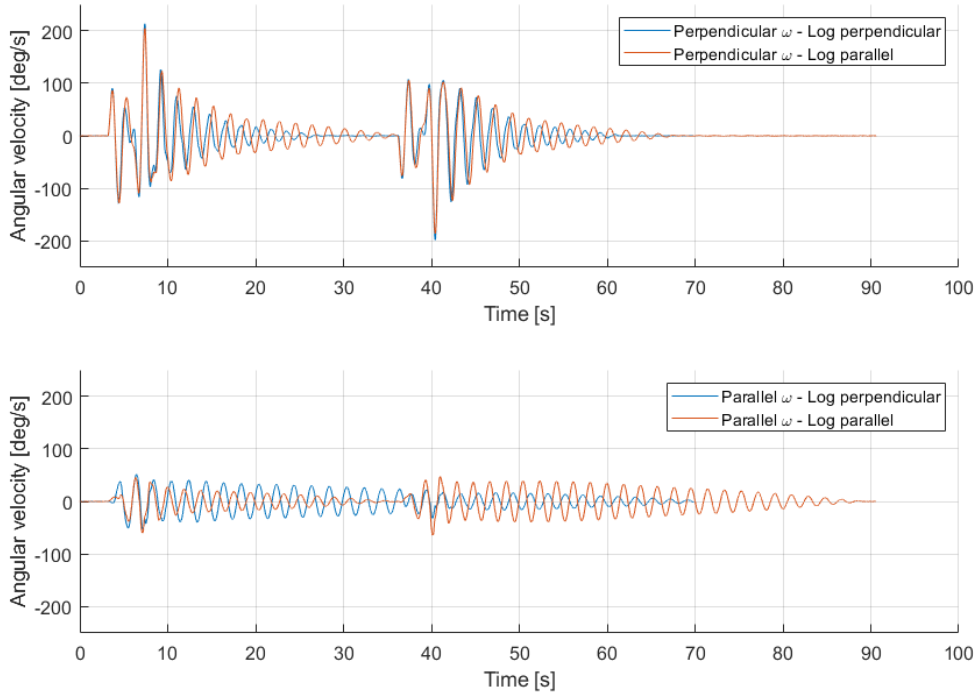

Figure 4.4. *Comparison of swaying with grapple rotation such as log is parallel and perpendicular to crane with slewing test scenario*

In perpendicular direction, amplitude of swaying does not change but small increase in swaying frequency is detectable. More significant changes are seen in parallel direction. However, in slewing it is the minor swaying direction and thus, it has to be studied also in tip x movement direction. Figure 4.5 presents the results for different grapple orientation when tip x test scenario is applied.

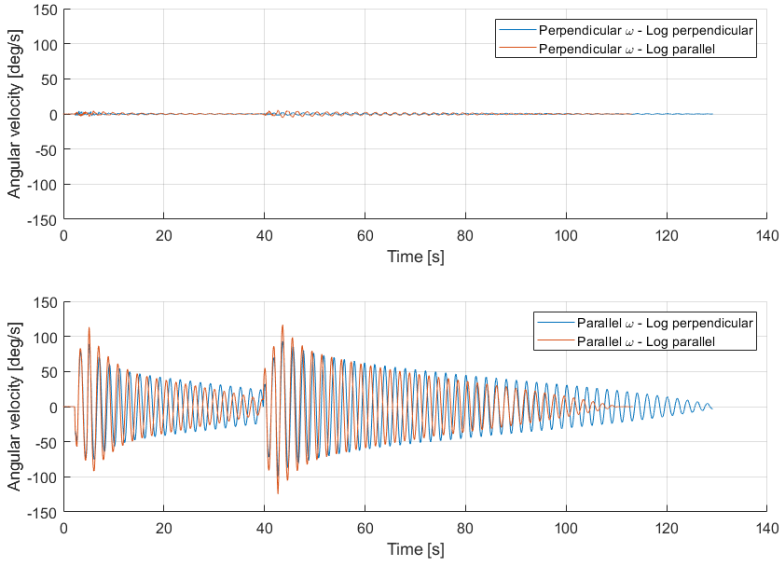

Figure 4.5. *Comparison of swaying with grapple rotation such as log is parallel and perpendicular to crane with tip x test scenario*

Similar changes in natural frequency is also seen when tip x is the movement direction. When grapple is turned 90 degrees to have log perpendicular to crane, natural frequency of parallel swaying is decreased. However, the change is small as it was with perpendicular swaying direction.

In addition to rotation of the grapple, also grapple opening can change the grapple orientation. The test scenarios is done with closed, partly open and fully open grapples. In all cases, the swaying is recorded. Figure 4.6 presents the effects of grapple opening to swaying.

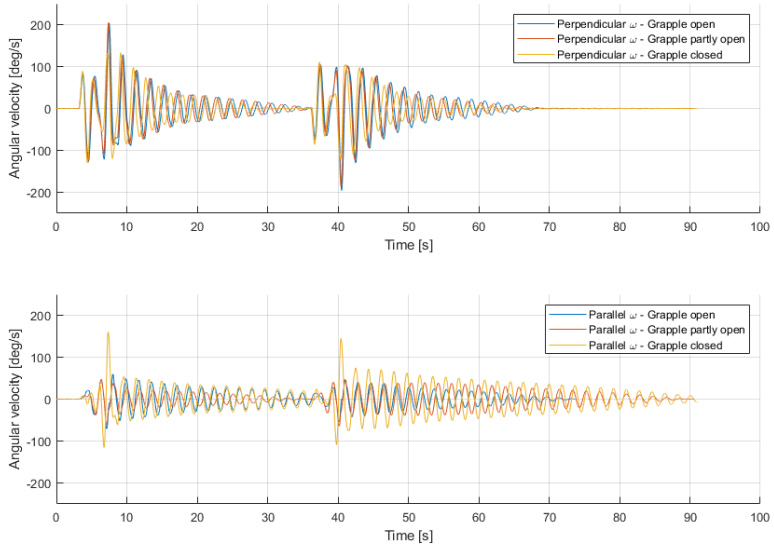

Figure 4.6. *Effect of grapple opening to swaying with slew test scenario*

As was noticed with rotated grapple, the main difference is seen in natural frequency of swaying. Between partly and fully open grapples there is no significant difference but closed grapple has higher natural frequency as the open grapple. In parallel swaying with closed grapple, also high starting peak is noticed. Similar high peak is however not seen in figure 4.7 where results for tip x test scenario is presented.

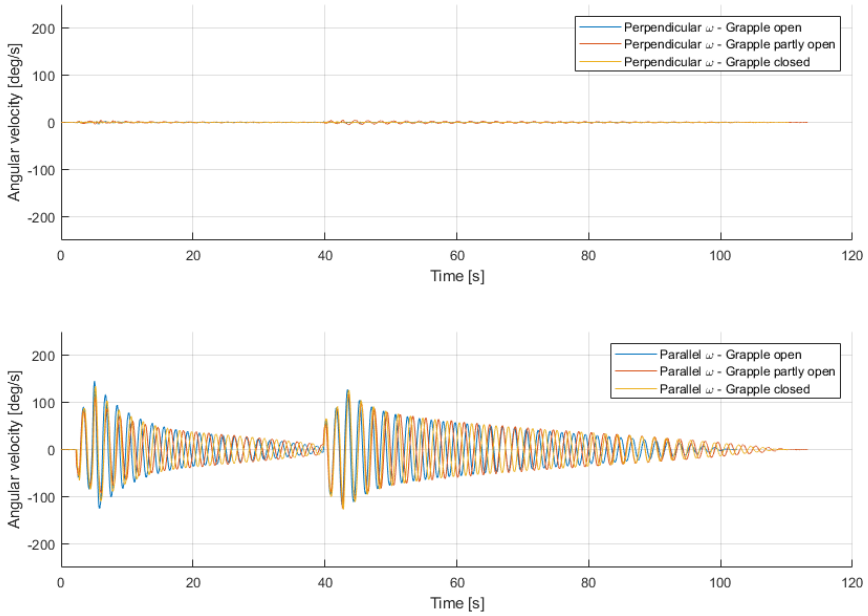

Figure 4.7. *Effect of grapple opening to swaying with tip x test scenario*

In parallel swaying when moving tip in x direction, only minor difference in natural frequencies is detected. As an conclusion from all tests related to grapple orientation can be said that the effects are minor and are mostly affecting the natural frequency when grapple is swaying freely. During transient, the behaviour of differently oriented grapples is similar.

4.3 Test scenario results for slewing movement

This subsection presents the results for RM shapers in tables 3.4, 3.5 and 3.6 that are designed to filter slewing command. The test scenario was presented in subsection 4.1. The resulting filtered positive part of the command is presented in figure 4.8 for RM shapers in table 3.4.

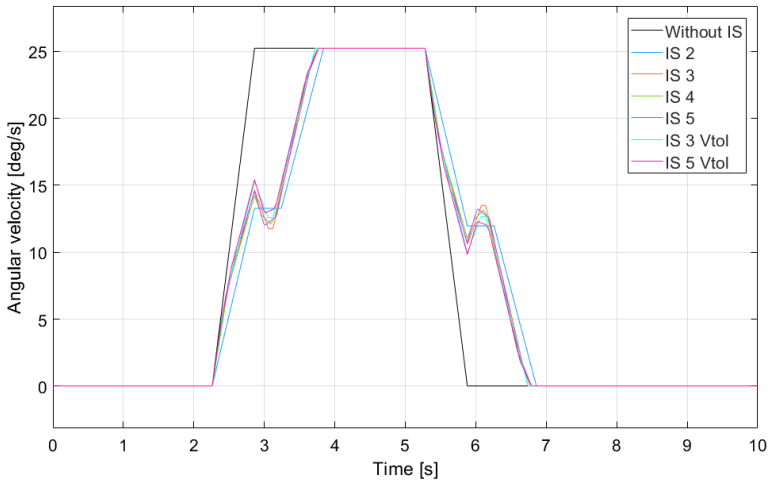

Figure 4.8. *Unmodified slewing test scenario command and filtered commands with RM shapers*

In figure 4.8, only the positive part of the velocity command is presented. As the original negative command is similar as the positive command, same command shape is seen also with the negative velocities. Excluding the 2 impulse RM shaper, all of the commands are close to each other. All of these commands causes a quick deceleration bump in the middle of acceleration. With 2 impulses, this is not possible and thus, the command has flat constant velocity phase in the middle of acceleration period. It is noticeable that with impulse number higher than 2, the command is slightly faster than with 2 impulses. Allthough, the difference is only approximately hundred milliseconds.

Test scenario with the RM shaper commands of figure 4.8 is then applied on the machine. Figure 4.9 shows the resulted swaying of grapple.

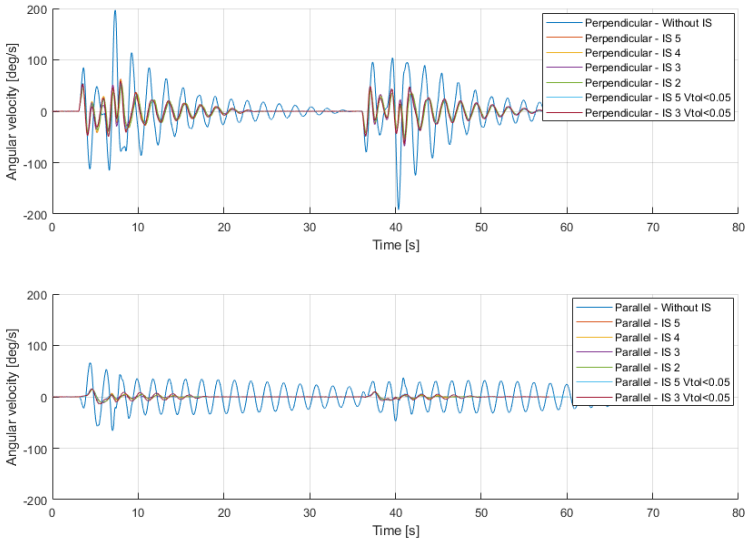

Figure 4.9. *Comparison between swaying on test sequence without input shaping and with different RM shapers*

All of the designed RM shapers are capable of reducing most of the swaying. At this point, the lack of slewing velocity to follow the command (see figures 4.1 and 4.2) has to be remembered. To be able to get full attenuation of swaying, the velocity has to follow the filtered command perfectly. Even with the presented performance of slewing, all of the RM shapers reduce most of the swaying. Also, the oscillations in the velocity when movement is stopped, causes some swaying (see figures 4.1 and 4.2). In addition to swaying angular velocities, it is important to address measured position and velocity of slewing which are presented in figure 4.10.

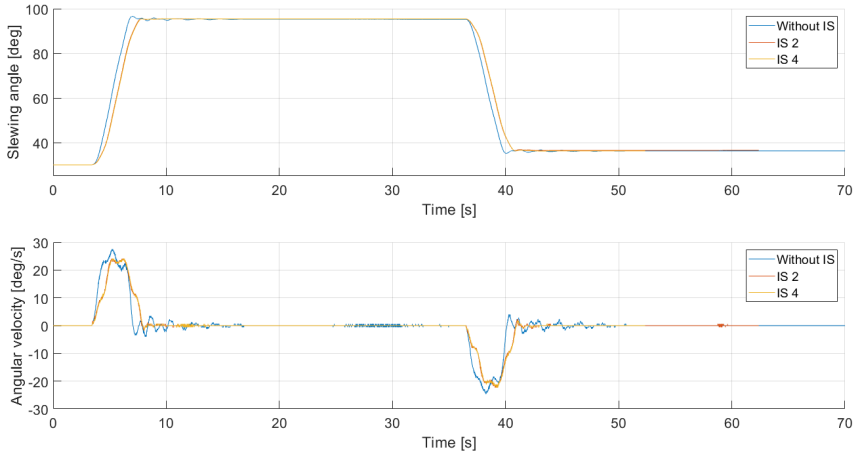

Figure 4.10. *Comparison between slewing angle and angular velocity without and with input shaping*

The figure 4.10 presents results only without RM shaper and with 2 and 4 impulse RM shapers to have easier comparison between the results. Between different tests, some fluctuation around starting point of 30 degrees exists. These fluctuation are neglected and the starting angle is set to 30 degrees for all tests. Noticeable is how similar the measured velocities are with 2 and 4 impulse RM shapers. Also, the delay of RM shaper is seen in the velocity. In slewing angle, travelled distance with and without input shaper are close to each other. However with input shaping, it takes longer time to reach the final position.

In addition, RM shapers were designed using erroneous natural frequency and damping ratio. Test scenario is also applied for these to study the robustness of RM shapers. As was noticed in subsection 4.2, the orientation of the grapple affects natural frequency of swaying. Therefore, it is important that RM shapers can tolerate some error in the natural frequency to reduce the swaying also in these situations. Also, the grapple is used to pick up logs which will change the center of the mass of grapple. Due to the current measurement system, tests with log was not possible. However, the change in center of the mass will affect the natural frequency and damping of the grapple.

At first, results with +10% error in natural frequency is presented in figure 4.11. To be

able to better compare the difference with and without error, swaying with 2 impulse RM shaper without error is presented in the following figures.

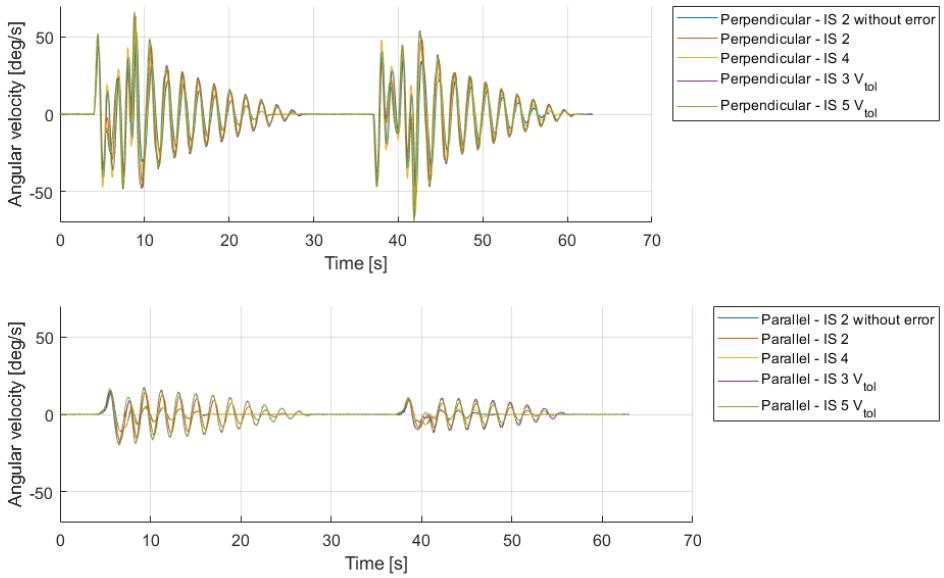

Figure 4.11. *Test scenario for slewing with table 3.5 input shapers that has +10% error in natural frequency*

Also, -10% error in natural frequency is tested and results presented in figure 4.12.

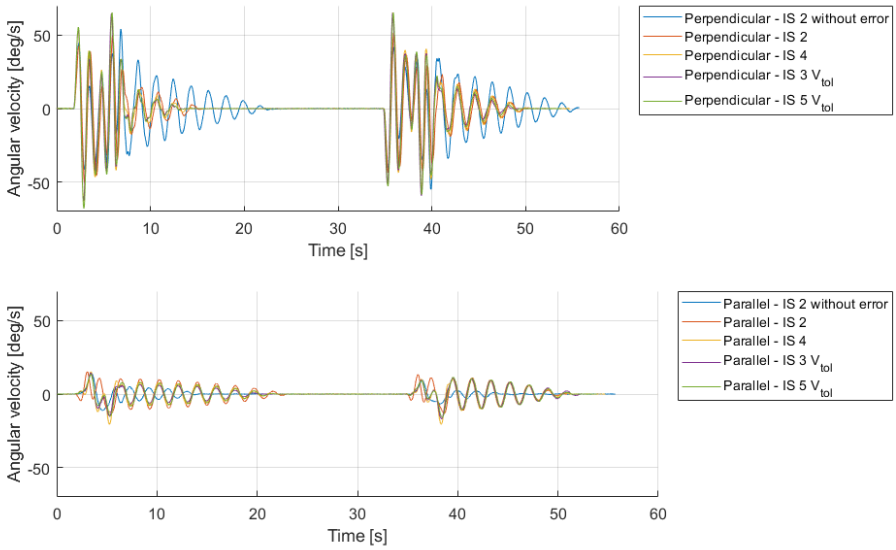

Figure 4.12. *Test scenario for slewing with table 3.5 input shapers that has -10% error in natural frequency*

The tested RM shapers with error in natural frequency are presented in table 3.5. In both cases, reduction in swaying is significant and $\pm 10\%$ error seems to not affect the performance of RM shapers. Also in both cases, all of the designed RM shapers perform equally well.

Second case is to add error in to damping factor. With the orientation of the grapple, damping of the grapple remained mostly the same in all cases. However, in previously mentioned case where log is in the grapple, the situation might change. Therefore, it is also important to test the robustness towards erroneous damping ratio. Figures 4.13 and 4.14 shows the results where 5 times higher and smaller damping ratio is used in the RM shaper design. Resulting RM shapers are presented in table 3.6

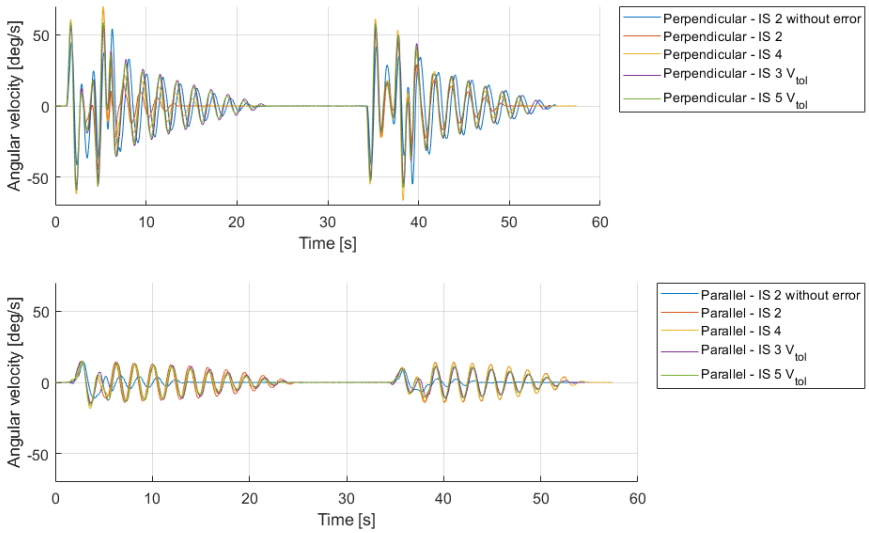

Figure 4.13. *Test scenario for slewing with table 3.6 input shapers that has 5 times larger damping ratio*

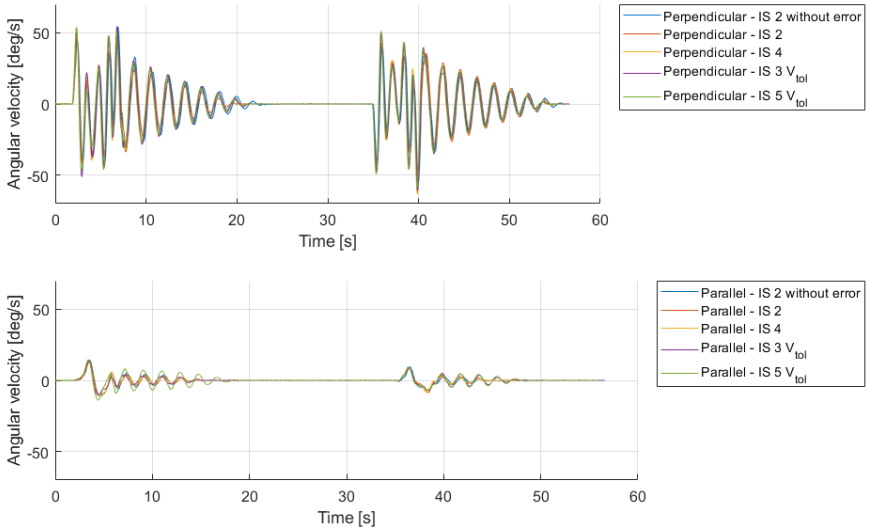

Figure 4.14. *Test scenario for slewing with table 3.6 input shapers that has 5 times smaller damping ratio*

In both cases, the results are close to each other and swaying is reduced significantly. The results are also close to what is gotten without error in damping ratio. Therefore, with

5 times higher or smaller natural frequency, the RM shaper is capable of reducing the swaying.

4.4 Test scenario results for tip near-far movement

In subsection 4.3, test scenario was applied for slewing and the resulting swaying for RM shaper with and without error presented. Similarly, this subsection presents the test scenario results for tip x movement. At first, figure 4.15 presents results without RM shaper and with RM shapers that has different amount of impulses.

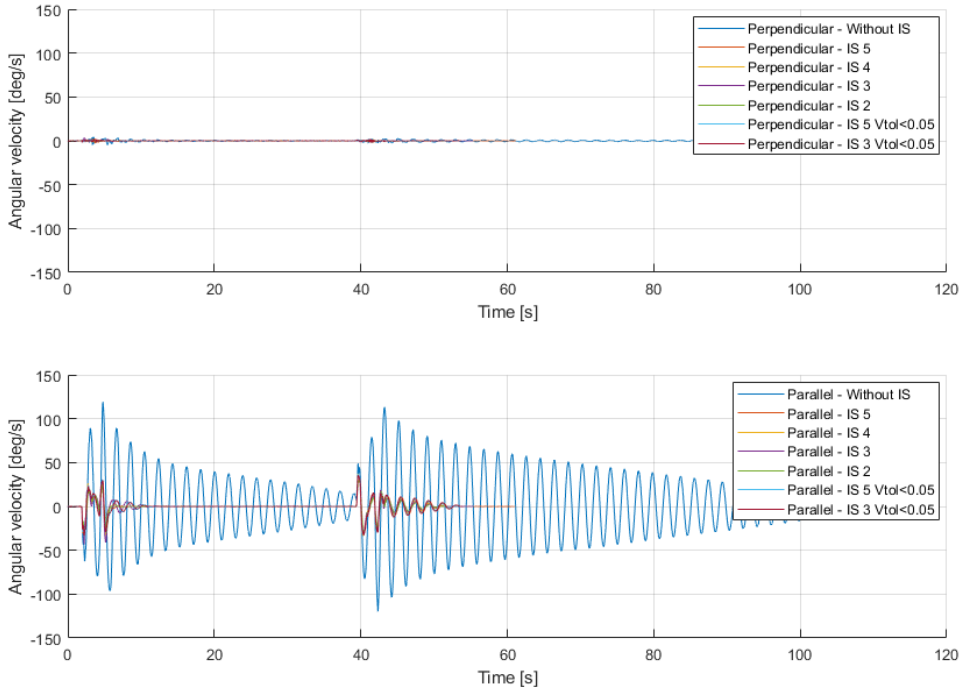

Figure 4.15. *Comparison between swaying on test sequence without input shaping and with different RM shapers*

As good reduction of swaying was seen with filtered slewing angular velocity input, with tip x almost all of the swaying is attenuated. Only some swaying is observed during transient when crane is either accelerated or decelerated which is due to the first part of RM shaper command. The caused swaying is then attenuated with the remaining parts of the RM shaper. In subsection 2.5, this was explained to be the main idea of input shaping. The effect input shaping has on position and velocity in x-direction is presented in figure 4.16.

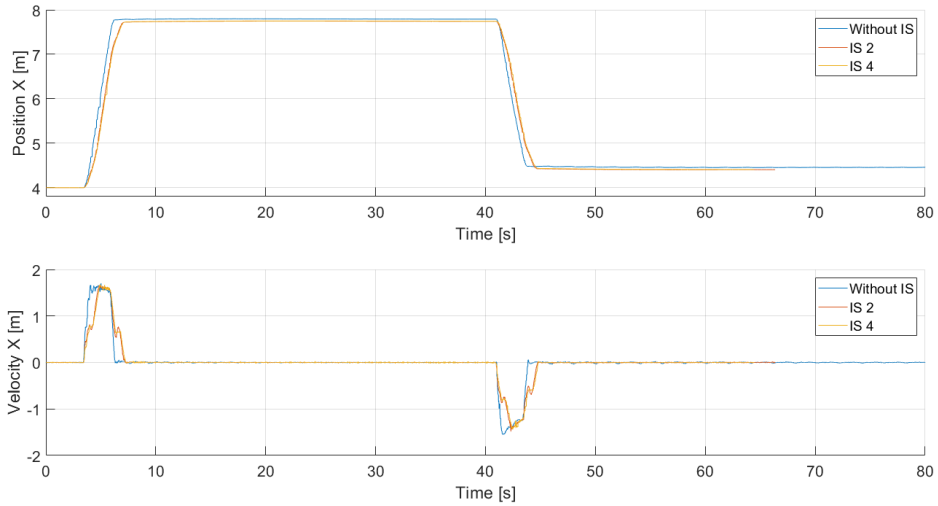

Figure 4.16. *Comparison between position and velocity of tip in x-direction without and with input shaping*

The starting position of tip in x-direction is set to four meters measured from the base of the crane. Between different tests, small fluctuation in starting positions exist. For comparison purposes, starting points are set equally to four meters and the fluctuation neglected. The delay of RM shaper is clearly seen in resulting velocity of the tip. In position, the tip travels close to equal distance with and without RM shaper. However with RM shaping, this takes a longer time equal to the delay of RM shaper.

As effect of error in the design parameters of RM shaper was investigated with slewing, similarly $\pm 10\%$ error in natural frequency and five times higher and smaller damping ratio are tested with tip x also. The tested RM shapers are presented in tables 3.5 and 3.6. Figures 4.17 and 4.18 presents the results with erroneous natural frequency.

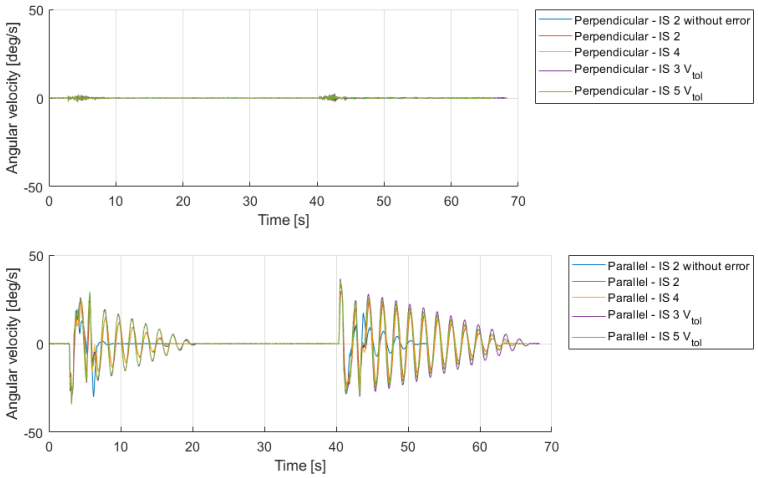

Figure 4.17. *Test scenario for Tip x with table 3.5 input shapers that has +10% error in natural frequency*

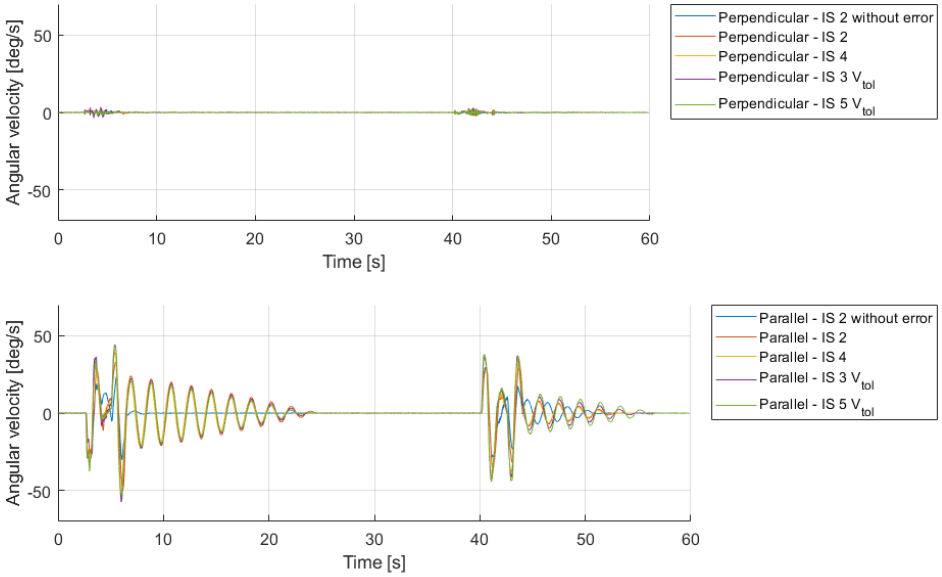

Figure 4.18. *Test scenario for Tip x with table 3.5 input shapers that has -10% error in natural frequency*

For tip x, performance of RM shaper deteriorate when error is added to natural frequency. However, major of the swaying is still attenuated. With positive error, negative command impulse (tip is moved towards the base) causes higher swaying than with negative error. In addition, also increased and decreased damping ratio is studied with tip x test scenario. Results are shown in figures 4.19 and 4.20

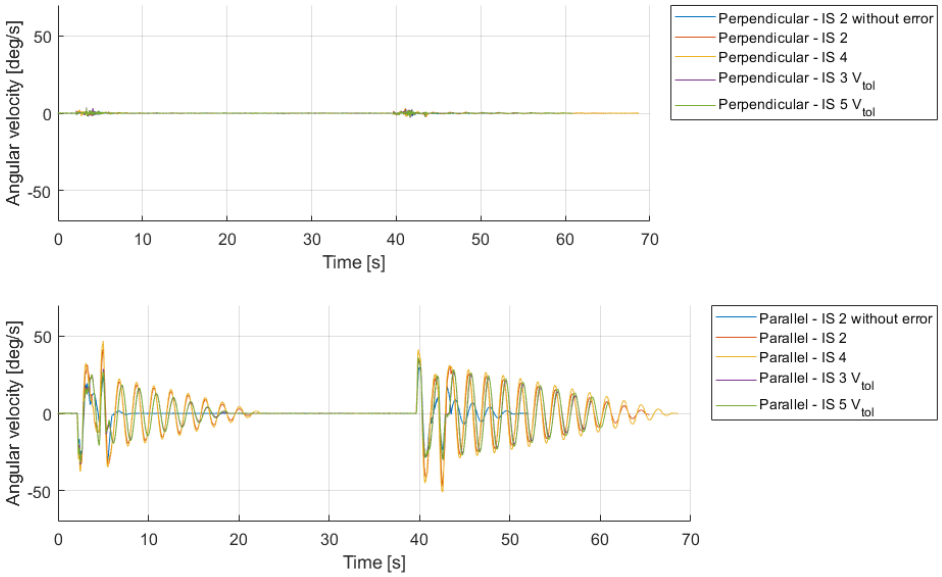

Figure 4.19. *Test scenario for Tip x with table 3.6 input shapers that has 5 times larger damping ratio*

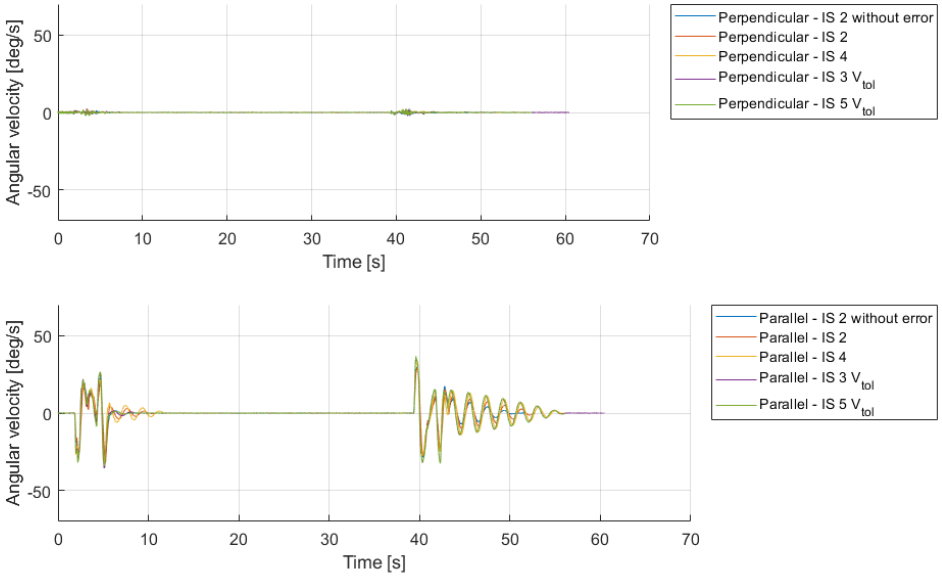

Figure 4.20. *Test scenario for Tip x with table 3.6 input shapers that has 5 times smaller damping ratio*

Compared to error in natural frequency, swaying is increased equal amount when damping is 5 times higher. With decreased damping however, no significant difference is detected. As a conclusion, in all cases where error is applied, RM shaper is attenuating major of the swaying.

5. CONCLUSION AND OUTLOOK

In this thesis, input shaping method was used to prevent swaying of forest machine grapple. More precisely, reduced modification (RM) shaper was implemented and tested with real forest machine. Inexperienced operator easily excite swaying in the grapple which mostly decrease productivity and efficiency but also safety. Therefore, controlling the crane without excessive swaying is important.

During the thesis, the aim was to answer the following research questions.

- To what extend can the grapple swaying be reduced with input shaping?
- How does changes in grapple orientation affect dampening ability of input shaping?
- How does parameter uncertainty of grapple affect the performance of input shaping?

Test results showed that input shaping can be used to prevent grapple swaying. In tested movement directions of tip near-far and slewing, major part of swaying was attenuated. Especially in near-far movement, almost all of the swaying caused by movement of tip was successfully attenuated with input shaping. With slewing, deterioration in performance of input shaping was caused by the incapability of actual slewing angular velocity to follow quick changes in command. Despite of that, attenuation of swaying was still significant.

Input shaping method is based on knowledge of the system natural frequency and damping ratio. Therefore, parameter uncertainties were point of interest. From the dynamic model of the grapple, physical parameters affecting the swaying are the two lengths l_1 and l_2 between grapple joints and center of mass of grapple (see figures 3.1 and 3.2), friction coefficients of grapple joints, and mass of the grapple. These parameters can be affected by changing the grapple orientation (opening and rotation) or increasing the mass. Due to the implemented measurement system, testing with a log as additional weight was not possible. Therefore, only changes in grapple orientation was tested. It was discovered that grapple orientation has only minor effect on natural frequency of swaying.

Parameter uncertainty was also studied by introducing an error in modelled natural frequency and damping ratio. Optimization problem of input shaping was then solved for the erroneous parameters. With natural frequency, $\pm 10\%$ error was tested with both

movement directions and results showed that compared to error free case, the swaying increased only a little. With slewing, the changes were smaller due to performance issues mentioned previously. With near-far movement, the swaying was increased but still major part is attenuated. In conclusion, the performance was not excessively deteriorated, when $\pm 10\%$ error in natural frequency occurred.

In second case, five times smaller and higher damping ratio was tested. Also in this case, swaying was increased only a little but the error in the damping ratio was considerably large. Therefore, since the performance of input shaper remained satisfactory, the damping ratio do not have as high role as natural frequency in the optimization problem of input shaping.

However, input shaping method has especially one major drawback. The main idea of input shaping is to delay parts of command signal which purpose is to cancel out the swaying. Therefore, a delay to the command is introduced that operator observes during the crane operation. Even though, the purpose of reduced modification (RM) shaper was to minimize the modification made to original command, it is easily observed by the operator. Also, the optimization problem of input shaping uses the system parameters to determine the amount of delay. Thus with input shaping, the amount of delay remains close to a constant and can be affected only slightly.

During the thesis, also dynamical model of the grapple was formed. However due to the measurement system, uncertainty in identified parameters exist. In future, more accurate measurement system should be implement to further refine the grapple model. Based on the grapple model, estimator based feedback control for sway reduction could be implemented. With anti-sway feedback control, it could be possible to reduce the modification that input shaping does to control signal. However, this would require a implementation of a new measurement system and controller.

During this thesis, operator aspect was not addressed. For future considerations, next obvious step could be to test input shaping with operators that have different experience levels. The results with traditional crane control without input shaping could be then compared with the ones gotten with crane control with input shaping. The hypothesis here is that for inexperienced operators, the input shaping might be useful when learning efficient way of operating the crane. For inexperienced operators, input shaping could reduce the cognitive load since they do not need to worry about excessive swaying of grapple. For experienced operators, however, there probably is no need for sway reduction algorithm since they are already familiar how to operate the crane fluently. Besides that, the delay introduced to the command is unwanted and probably makes the crane movements feel sluggish for the experienced operators. Still, the effect of input shaping to productivity between different experience level operators could be thing to consider in future.

Operator aspect studies would require picking up logs and moving them to and from

load space. During the thesis, additional weight that log adds to grapple was not tested due to restrictions of the measurement system. However, the additional weight probably deteriorates the performance of input shaping. Testing with load would be then one key aspect to see if the designed input shaper is capable of reducing the swaying also when the grapple is not empty. Also, the place where log is grabbed, will affect the center of mass of the grapple. Thus, there remains plenty of different scenarios to consider with load.

Another potential application for sway reduction algorithm is with automated movements of crane. With automated movements, the grapple swaying is detrimental since there does not exist any measurements from which the control system could detect the swaying. Therefore, input shaping could be used to prevent the swaying. Also with automated movements, there does not exist similar issues with the delayed command as does with human operator.

REFERENCES

[1] R. Parker, “Forestry automation and robotics.”, *New Zealand journal of forestry (New Zealand Institute of Forestry)*, vol. 1, no. 63, pp. 38–40, 2018.

[2] D. Ortiz Morales, S. Westerberg, P. X. La Hera, U. Mettin, L. Freidovich, and A. S. Shiriaev, “Increasing the level of automation in the forestry logging process with crane trajectory planning and control: Increasing the level of automation in the forestry logging.”, *Journal of field robotics*, vol. 31, no. 3, pp. 343–63, 2014.

[3] S. Fodor, C. Vázquez, L. Freidovich, and N. Sepehri, “Towards oscillation reduction in forestry cranes.”, *BATH/ASME 2016 Symposium on Fluid Power and Motion Control, FPMC 2016.*, 2016.

[4] M. H. I. Ishak, Z. Mohamed, and R. Mamat, “Anti-sway control schemes of a boom crane using command shaping techniques.”, *Jurnal teknologi A, Pembuatan, bahan termaju, tenaga dan pengangkutan.*, 2014.

[5] J. Kalmari, J. Backman, and A. Visala, “Nonlinear model predictive control of hydraulic forestry crane with automatic sway damping”, *Computers and electronics in agriculture.*, no. 109, pp. 36–45, 2014.

[6] S. Fodor, C. Vazquez, and L. Freidovich, “Automation of slewing motions for forestry cranes.”, *International Conference on Control, Automation and Systems (ICCAS). Institute of Control, Robotics and Systems - ICROS; 2015.*, pp. 796–801, 2015.

[7] H. Omar and A. Nayfeh, “Anti-swing control of gantry and tower cranes using fuzzy and time-delayed feedback with friction compensation.”, *Shock and vibration.*, vol. 2, no. 12, pp. 73–89, 2005.

[8] K. Hong, C. Huh, and K. Hong, “Command shaping control for limiting the transient sway angle of crane systems.”, *International journal of control, automation, and systems.*, vol. 1, no. 1, pp. 43–53, 2003.

[9] A. Kaneshige, T. Miyoshi, and K. Terashima, “The development of an autonomous mobile overhead crane system for the liquid tank transfer.”, *In: 2009 IEEE/ASME International Conference on Advanced Intelligent Mechatronics.*, pp. 630–5, 2009.

[10] R. Sato, Y. Noda, T. Miyoshi, *et al.*, “Operational support control by haptic joystick considering load sway suppression and obstacle avoidance for intelligent crane.”, *In: 2009 35th Annual Conference of IEEE Industrial Electronics.*, pp. 2301–7, 2009.

[11] M. Ahmad, F. Misran, M. Ramli, and R. Raja Ismail, “Experimental investigations of low pass filter techniques for sway control of a gantry crane system.”, *In: 2010 2nd International Conference on Electronic Computer Technology.*, pp. 1–4, 2010.

[12] E. Arnold, O. Sawodny, J. Neupert, and K. Schneider, “Anti-sway system for boom cranes based on a model predictive control approach.”, *Mechatronics (Oxford).*, no. 77, pp. 102 599–. 2021.

[13] J. Montonen, N. Nevaranta, M. Niemelä, and T. Lindh, “Comparison of extrainsensitive input shaping and swing-angle-estimation-based slew control approaches for a tower crane”, *Applied sciences.*, vol. 12, no. 12, pp. 5945–, 2022.

[14] H. Omar and A. Nayfeh, “Gain scheduling feedback control of tower cranes with friction compensation.”, *Journal of vibration and control.*, vol. 2, no. 10, pp. 269–89, 2004.

[15] Z. Masoud, A. Nayfeh, and A. Al-Mousa, “Delayed position-feedback controller for the reduction of payload pendulations of rotary cranes”, *Journal of vibration and control.*, vol. 1-2, no. 9, pp. 257–77, 2003.

[16] J. Potter and W. Singhose, “Design and human-in-the-loop testing of reduced-modification input shapers.”, *IEEE transactions on control systems technology.*, vol. 4, no. 24, pp. 1513–20, 2016.

[17] A. Abe and K. Okabe, “Antisway control for a rotary crane by using evolutionary computation.”, *Journal of robotics and mechatronics.*, vol. 5, no. 28, pp. 646–53, 2016.

[18] K. J. Jensen, M. K. Ebbesen, and M. R. Hansen, “Anti-swing control of a hydraulic loader crane with a hanging load.”, *Mechatronics (Oxford).*, no. 77, pp. 102 599–. 2021.

[19] K. Aström and R. Murray, “Feedback systems: An introduction for scientists and engineers.”, *New Jersey: Princeton University Press*, 2010.

[20] W. Singhose, “Command shaping for flexible systems: A review of the first 50 years”, *Int J Precis Eng Manuf, 2009, 10(4): 153– 168.*, 2009.

[21] K. Ogata, “Modern control engineering. 5th ed.”, *Upper Saddle River (NJ): Pearson*, 2010.

[22] A. Mandal, “Introduction to control engineering: Modeling, analysis and design.”, *New Delhi: New Age International P ltd., Publishers*, 2006.

[23] R. Dorf and R. Bishop, “Modern control systems. thirteenth edition.”, *Harlow: Pearson*, 2017.

[24] S. Burns, “Advanced control engineering”, *Elsevier Science Technology*, 2001.

[25] A. Sage and J. Melsa, “System identification”, *New York Academic Press*, 1971.

[26] M. Golnaraghi and B. Kuo, “Automatic control systems, tenth edition /. 10th edition.”, *New York, N.Y: McGraw-Hill Education*, 2017.

[27] N. Singer and W. Seering, “Preshaping command inputs to reduce system vibration.”, *ASME J. Dyn. Syst., Meas., Control, vol. 112, no. 1, pp. 76–82*, 1990.

[28] M. Tokhi and A. Azad, “Flexible robot manipulators modelling, simulation and control.”, *London: Institution of Engineering and Technology*, 2008.

[29] W. Singhose, W. Seering, and N. Singer, “Input shaping for vibration reduction with specified insensitivity to modeling errors.”, *In: Proceedings of the Japan/USA Symposium on Flexible Automation.*, pp. 307–13, 1996.

[30] T. Singh and S. Vadali, “Robust time-delay control.”, *Journal of dynamic systems, measurement, and control.*, vol. 2A, no. 115, pp. 303–6, 1993.

[31] L. Pao, “Multi-input shaping design for vibration reduction.”, *Automatica (Oxford).*, vol. 1, no. 35, pp. 81–9, 1999.

[32] J. Kalmari, H. Hyyti, and A. Visala, “Sway estimation using inertial measurement units for cranes with a rotating tool.”, *IFAC Proceedings Volumes.*, vol. 10, no. 46, pp. 274–9, 2013.

[33] J. Craig, “Introduction to robotics: Mechanics and control. 3rd ed.”, *Upper Saddle River (NJ): Prentice Hall*, 2005.

[34] M. Bock and A. Kugi, “Real-time nonlinear model predictive path-following control of a laboratory tower crane”, *IEEE transactions on control systems technology.*, vol. 4, no. 22, pp. 1461–73, 2014.